

*Department of Construction Sciences*  
**Solid Mechanics**

ISRN LUTFD2/TFHF-18/5227-SE(1-81)

# **Compression analysis of primary and secondary package**

Master's Dissertation by

**Filip Lotzke**  
and  
**Johannes Nyberg**

Supervisors:

M. Sc. Andreas Larsson, Tetra Pak AB  
Adj. Prof. Johan Tryding, Div. of Solid Mechanics

Examiner:

Prof. Mathias Wallin, Div. of Solid Mechanics

Copyright © 2018 by the Division of Solid Mechanics,  
Filip Lotzke and Johannes Nyberg

Printed by Media-Tryck AB, Lund, Sweden

For information, address:

Division of Solid Mechanics, Lund University, Box 118, SE-221 00 Lund, Sweden

Webpage: [www.solid.lth.se](http://www.solid.lth.se)



# Acknowledgements

The research presented in this Master Thesis was carried out at Tetra Pak in Lund in cooperation with the Division of Solid Mechanics at Lund University, Sweden, during January to June 2018.

At first we would like to express our deepest gratitude to our two supervisors, M.Sc Andreas Larsson and Adj. Prof. Johan Tryding. Andreas has always taken his time to share valuable insights, given us feedback when needed, helped us keep our spirits high when times were tough and always met us with a warming smile. Johan has shared his knowledge about paperboard and given us valuable feedback for our report. Thank you for making this thesis fun and interesting to work with. Without you two this Master thesis would never had been finish.

A big and special thanks to Jonas Gagner for always taking his time answering our questions pedagogically and often the same question over and over again. Without you none of the simulations would converge.

Patrik Landroth has shared his knowledge within Tetra Recart and helped us ordering packages for the physical tests.

Eskil Andreasson, Hanna Eliasson and Johan Nordgren are only a few at Tetra Pak who have helped us and showed interest in our progress.

William Dahlgren and Anes Sestic for showing us a different perspective and always waiting for us in the lunch queue.

Lastly, we would like to thank our families for all their love and support. We would not be here if it were not for them.

Thank you all for the joyful time at Tetra Pak.

Filip Lotzke and Johannes Nyberg  
Lund, May 2018





# Abstract

The aim of this thesis was to investigate how packages, both primary and secondary, behave under transportation. Before a full analysis of a pallet distribution can be fully understood the understanding of the separate packages is required. This thesis contributes with great knowledge and understanding of how a primary and secondary package behaves during top load compression.

Tetra Pak is a global leader in the food & packaging industry and in order to maintain this market position, continuous investments in new technologies is of great importance. Finite Element analysis is one of these technologies which enables more understanding of the manufacturing process and makes faster decision based on well-grounded results possible.

This thesis is divided into two parts; Experimental tests and Finite Element Modeling, FEM. The experiment is in detailed described, evaluated and discussed using relevant theory, statistical analysis and observations. Several modeling approaches have been reviewed and two final finite element models is presented.

The information collected from the experimental tests in combination with engineering reasoning have contributed to an increased understanding of which parameters are of great importance to capture the physical behavior on a macro-scale. The results from the finite element modeling indicates an modeling approach that capture these behaviors in accordance to the observations and analysis.

The result from the work done in this thesis have a foundation for continuous improvements. Future difficulties have been highlighted but a workable approach is presented.

*Keywords:* Box Compression, Top Load, Corrugated Board, Finite Element Simulations, ABAQUS/Explicit



# Sammanfattning

Målet med denna avhandling var att undersöka hur pappersförpackningar, både primär och sekundär, beter sig under transport. Innan en storskalig analys av en pall distribution kan genomföras behövs kunskap av hur enskilda förpackningar beter sig. Denna avhandling bidrar med nyttig kunskap och förståelse av hur en primär förpackning och en sekundär förpackning påverkas av kompressionslaster.

Tetra Pak är en framstående aktör inom mat och förpackningsindustrin och för att behålla sin ledande roll, behövs kontinuerliga investeringar i nya tekniker. Finita element analyser är en av dessa värdefulla tekniker som underlättar förståelse av tillverknings processen och bidrar till att snabbare beslut kan tas.

Denna avhandling är uppdelad i två delar; Fysiska test och Finita Element Modeller- ing, FEM. Experimenten är beskrivna detaljerat och har utvärderats och diskuterats utifrån relevant teori. Statistisk analys används och samtliga observationer framförs. Olika modeleringstekniker har användts och resultatet är presenterat som två mod- eller som överensstämmer väl med verkliga tester.

Informationen som insamlats från de experimentella testerna i kombination med lo- giska resonemang har bidragit till en ökad förståelse om vilka faktorer som är av yttersta vikt för att kunna fånga de fysiska beteenden på en övergriplig nivå. Re- sultaten från simuleringarna hänvisar till en modelleringsmetod som fångar viktiga beteenden i hänsyn till observationerna och analysen.

Resultaten från denna avhandling har en grund för fortsatta förbättringar. Framtida svårigheter har uppmärksammas och en fortsatt väg framåt har presenterats.

*Keywords:* Box Compression, Top Load, Corrugated Board, Finite Element Simu- lations, ABAQUS/Explicit



# Contents

<b>1</b>	<b>Introduction</b>	<b>1</b>
1.1	Background . . . . .	1
1.2	Objectives . . . . .	1
1.3	Paperboard . . . . .	2
1.4	Tetra Recart . . . . .	3
1.5	Corrugated Board . . . . .	4
1.6	Notations . . . . .	5
<b>2</b>	<b>Package Transportation</b>	<b>7</b>
2.1	Background . . . . .	7
2.1.1	Standards . . . . .	7
2.2	Pallet distribution . . . . .	7
2.2.1	Drop test . . . . .	8
2.2.2	Horizontal impact test . . . . .	8
2.2.3	Random vibration test . . . . .	8
2.2.4	Recommendations . . . . .	8
2.3	Secondary package . . . . .	9
2.4	Primary package . . . . .	9
2.5	Computational simulation . . . . .	9
<b>3</b>	<b>Theory</b>	<b>11</b>
3.1	Box Compression . . . . .	11
3.2	Corrugated Board . . . . .	11
3.3	Continuum Mechanics . . . . .	12
3.3.1	Hill's Yield Criterion . . . . .	12
3.3.2	Calibration of paperboard data to Hill plasticity model . . . . .	14
3.3.3	Kinematics of large deformations and small strains . . . . .	16
3.4	Finite Element Model . . . . .	16
3.4.1	ABAQUS/Explicit . . . . .	16
3.4.2	Shell elements . . . . .	18
<b>4</b>	<b>3D Scanner Test</b>	<b>19</b>
4.1	Introduction . . . . .	19
4.2	3D Scan . . . . .	19
4.2.1	Samples . . . . .	19

4.2.2	Test Equipment . . . . .	19
4.2.3	Result . . . . .	20
4.2.4	Analysis . . . . .	21
<b>5</b>	<b>Top Load Compression Tests</b>	<b>23</b>
5.1	Introduction . . . . .	23
5.1.1	Samples . . . . .	23
5.1.2	Test Equipment . . . . .	23
5.2	Primary Package . . . . .	24
5.2.1	Method . . . . .	24
5.2.2	Result . . . . .	24
5.2.3	Analysis . . . . .	30
5.3	Secondary Package . . . . .	30
5.3.1	Method . . . . .	30
5.3.2	Result . . . . .	31
5.3.3	Analysis . . . . .	32
5.4	Secondary Unit . . . . .	33
5.4.1	Method . . . . .	33
5.4.2	Result . . . . .	33
5.4.3	Analysis . . . . .	36
<b>6</b>	<b>Finite Element Modeling in ABAQUS</b>	<b>37</b>
6.1	Introduction . . . . .	37
6.1.1	Material . . . . .	37
6.2	Geometry Dependent Rectangle . . . . .	38
6.2.1	Result . . . . .	38
6.2.2	Analysis . . . . .	39
6.3	Folded TRC Package . . . . .	40
6.3.1	Mesh . . . . .	40
6.3.2	The folding procedure . . . . .	41
6.3.3	Result . . . . .	42
6.3.4	Analysis . . . . .	43
6.4	Modified Geometry . . . . .	43
6.4.1	Modifications . . . . .	43
6.5	Final TRC Model . . . . .	44
6.6	Secondary package . . . . .	47
6.6.1	Introduction . . . . .	47
6.7	Secondary Unit . . . . .	50
6.7.1	Assembling . . . . .	50
<b>7</b>	<b>Top Load Compression Simulation</b>	<b>53</b>
7.1	Introduction . . . . .	53
7.1.1	Mass-scaling . . . . .	53
7.2	Primary Package Model . . . . .	53
7.2.1	Method . . . . .	53

7.2.2	Result . . . . .	54
7.2.3	Analysis . . . . .	58
7.2.4	Conclusions . . . . .	59
7.3	Secondary Package Model . . . . .	60
7.3.1	Method . . . . .	60
7.3.2	Result . . . . .	60
7.3.3	Analysis . . . . .	62
7.3.4	Conclusions . . . . .	63
7.4	Secondary Unit Model . . . . .	63
7.4.1	Method . . . . .	63
7.4.2	Results . . . . .	64
7.4.3	Analysis . . . . .	66
7.4.4	Conclusions . . . . .	67
<b>8</b>	<b>Discussion and Conclusions</b>	<b>69</b>
8.1	Summary of thesis . . . . .	69
8.2	Measurements discussion . . . . .	69
8.3	Modelling discussion . . . . .	70
8.4	Future work . . . . .	72
	<b>Appendices</b>	<b>77</b>
<b>A</b>	<b>Model data</b>	<b>78</b>
A.1	Bulk modulus . . . . .	78
<b>B</b>	<b>Pictures</b>	<b>79</b>





# Chapter 1

## Introduction

Tetra Pak is a world leading company in food processing and packaging solutions. Tetra Pak's motto "Protects what's good" reflects their vision to make food safe and available, everywhere. The company was founded in Lund, Sweden by Ruben Rausing in 1951. Tetra Pak is today located in more than 175 countries [1]. Their products are divided into mainly three categories, Packaging, Processing and Services. This thesis is done at the Packaging segment where the carton package Tetra Recart is a part of the portfolio. The package is designed to contain food and is also the product evaluated in this master thesis.

### 1.1 Background

Pallet distribution tests are very time consuming and expensive. Today's measured responses are binomial which requires a lot of tests to gain sufficient statistical confidence. Tetra Pak wants to increase the knowledge of which parameters and design principles that are important for a robust distribution solution. Distribution tests are today done late in projects which narrows the design space if issues are found. To fully understand a simulation of a new design pallet distribution is a future goal for Tetra Pak. To be able to perform these simulations and to understand the physics Tetra Pak needs more knowledge of how a primary package and secondary package behaves during simple compression.

To gain further knowledge this thesis will focus on gathering information from physical tests and comparing these with Finite Element models built in ABAQUS/Explicit of primary and secondary packages.

### 1.2 Objectives

To fully understand and simulate the physics in a pallet distribution test is a complex problem. Instead it is better to break down the problem into smaller blocks and understand these.

The goal of this master thesis is to understand these two building blocks.

1. Top load of a Primary package and a Secondary package. The objective is to understand how the packages behaves depending on different loads. And to find the buckling modes depending on the direction and magnitude of the compression force. Design FE-models that capture the result from the physical test.
2. Combine 16 Primary packages and a Secondary package into a Secondary unit. This will be taken into consideration when the first block is well understood. Perform physical test to validate the assembled FE-model.

### 1.3 Paperboard

The paperboard used at Tetra Pak is made from two different types of fibers, softwood and hardwood. Softwood is also called longfiber because of its length of 4-6 mm, the softwood adds strength to the paperboard. Hardwood also known as shortfiber because they are short and thick, length of 1 mm, is mixed to the paperboard to make a smooth surface for easier printing. Paperboard is an orthotropic material meaning the mechanical properties is different in the three specified direction seen in figure 1.1. The orthotropic behavior in paperboard is due to fibers are oriented in the manufacturing process. The three directions are machine direction (MD), cross direction (CD) and out of plane direction (ZD). Paperboard is an renewable and recyclable material and has valuable material properties such as high strength too weight ratio and easy foldability and cutability.

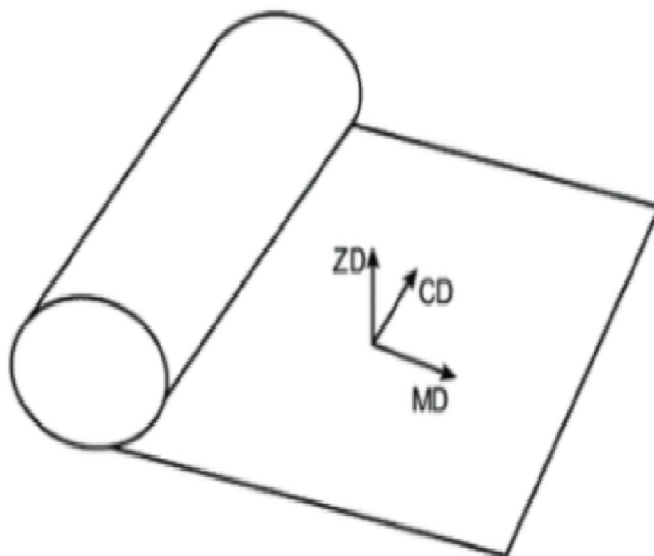


Figure 1.1: The orientation of the material directions.

## 1.4 Tetra Recart

During production Tetra Recart packages and its product is sterilized with steam to eliminate micro-bacteria growth. The package material consist of several different material plies all contributing with different material properties. The aluminum foil is present to protect the product from UV radiation and also for the sealing in the top and bottom. The polymer layers exist to protect the product, the paperboard from moisture and also working as adhesive material to stack the material plies together. See figure 1.2 for the material composition of a Tetra Recart package.



Figure 1.2: The material structures of an Tetra Recart package. [2]

To transport Tetra Recart packages to the retailers the primary package is packaged in secondary packages for protection and is stacked in a specific pattern on a pallet for stability, see figure 1.3. The pattern is designed to handle different pallet sizes, distribution routes and volume maximization.



Figure 1.3: Picture (a) shows different volumes of primary package, (b) secondary package containing 16 primary packages i.e. a secondary unit and picture (c) a pallet with secondary units interlocked in a special pattern. [2]

## 1.5 Corrugated Board

Corrugated board is used in Tetra Recart's secondary packages due to its high strength and board stiffness in relation to low price. However one of the unfavorable properties is its sensitivity to moisture making the material performance highly dependent on the ambient conditions. The most common form of corrugated board is the single-wall board, consisting of two liners that are bonded together by a wave shaped web called flute. Depending on the package size different flutes are used, they are characterized by a letter and the packages used by Tetra Pak either B- or C- flute is of interest. The letter quantifies the length of the fluting per unit length of the board. Below is an illustration of a small piece of corrugated board and its material orientations, see figure 1.4

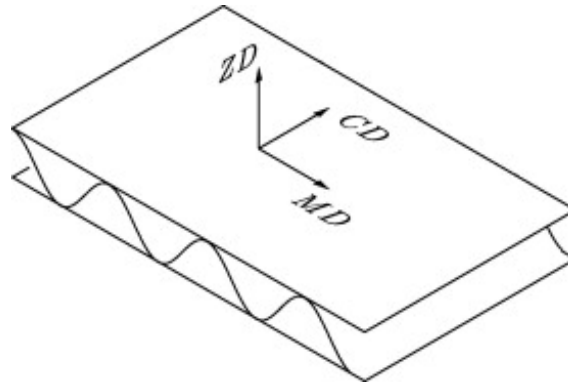


Figure 1.4: The material orientations of corrugated board.

The secondary package used for Tetra Recart have perforation in the corners for easier folding the perforation is evenly spaced with an approximate length of 10 mm.

## 1.6 Notations

Both tensor and matrix notations are used throughout this report, the following index free notations were used for the first and second order tensors

$m_i \leftrightarrow \mathbf{m}$	$M_{ij} \leftrightarrow \mathbf{M}$
First order	Second order
tensor	tensor

### Indices

All the mathematical expression in this report is referring to the material orientation MD, CD and ZD as 1, 2 and 3, respectively. Two examples is given below

$$\begin{aligned} E_{MD} &= E_1 \\ G_{MDCD} &= G_{12}. \end{aligned}$$

When dealing with corrugated board the layers in the composite is numbered 1, 2 and 3 for the top liner, flute and bottom liner, respectively. In combination with the material orientation the corrugated board notation is separated with a comma, an example is given below

$$G_{MDCD, bottomliner} = G_{12,3}.$$



# Chapter 2

## Package Transportation

This chapter contains the literature search collected at Tetra Pak and at other various information sites. The chapter is a discussion from a Tetra Pak perspective compared to the market taking international standards into consideration. The chapter is divided into subsection Pallet distribution, Secondary package and Primary package where each section describes a part of a transportation test.

### 2.1 Background

To be able to develop and design competitive packages that maintain its integrity and visual appeal throughout the distribution chain one must first understand the whole package chain. There is several companies and international standards to guide companies, such as Tetra Pak, with knowledge and help them simulate physical tests that should represent the reality. One must take consideration to every distribution chain is unique and the variety is large between countries, suppliers and distributors.

#### 2.1.1 Standards

Two of the most common test standards in package distribution testing are American Society of Testing Materials (ASTM International) and International Safe Transit Association (ISTA). The two test standards have developed several test to comply with the International Organization for Standardization (ISO) ICS 55.180.40 - *Complete, filled transport packages* [3]. The two standards are therefore not comparable due to the different setups. Some of the test method at Tetra Pak is based on the ASTM International D4169 - *Standard Practice for Performance Testing of Shipping Containers and Systems* [4].

### 2.2 Pallet distribution

Pallet distribution test is simulating the impact a pallet is received throughout the distribution chain. Drop and horizontal impact test simulates loading and unloading for transport, warehouse handling with forklift and acceleration/break during transport,

all scenarios that affects the pallet with a short impact. The Random vibration test should simulate the vibrations a pallet is received during transportation. Often the vibration appears from the road/rail structure or vibrations from machines. The test procedure combines the three test and an final evaluation of the packages is performed afterwards.

### **2.2.1 Drop test**

The drop test is a "raised edge test" according to the ASTM D4169 standard. Both the long and short side of a pallet is tested. The height of the drop is what differentiate the two standards, ASTM and ISTA, from each other.

### **2.2.2 Horizontal impact test**

The horizontal test is a pallet on a sledge with a small inclination, the sledge slide into a vertical wall simulating a Horizontal impact, according to ASTM D4169. However the small inclination makes the upper package layers of the pallet impact the vertical wall first representing an acceleration or a break. ISTA standards recommend a horizontal impact test with no inclination.

### **2.2.3 Random vibration test**

The vibration frequency is according to ISO 13355 standard and Tetra Recart is using a standard vibration profile ASTM 4728. Often in distribution to maximize the transportation volume more packages or pallets are stacked on top of each other. Addition to the current test is a static load on top of the pallet to simulate overstacked pallets. During transportation the pallet is affected both by road/machine vibration and acceleration/breaks. To better simulate this combination a "Rotary Vibration Test" can be used that include g-forces acting on the pallet from e.g. roundabouts.

### **2.2.4 Recommendations**

Additional test:

- "Static Load Vibration test" - To maximize the transportation volume more load is stacked on top of the pallet, this test consider the extra weight on the top.
- "Rotary Vibration test" - During transportation the pallet is affected both by road/machine vibration and acceleration/breaks simultaneous. Often the layers of packages have shifted from the original stacking pattern after transportation. The Rotary vibration test can add knowledge of which stacking pattern best suited for transportation.
- "G-force transportation test" - G-force affects the pallets in e.g. roundabouts this moves the layers of packages shifting the original pattern.



## 2.3 Secondary package

Tetra Recart do not perform test on secondary packages. One explanation is the test are well performed on the sub levels, primary package and pallet, the secondary packages are included and evaluated. Recommendation is to test box compression on secondary packages with corrugated board to collect information on how the BCR changes under different conditions.

## 2.4 Primary package

On primary package Tetra Pak performs multiple physical tests. The test includes, static compression, dynamic compression, drop test and evaluation of package appearance after transportation test to mention a few. The test are well performed and covers the whole spectrum.

## 2.5 Computational simulation

In Lönn and Navéd [5] a primary package is model and simulated under a drop test. In house Tetra Pak have several development reports of how to simulate primary package under different transportation test, they have also reports of computational models on pallet level, largely simplified. No full analysis of a pallet distribution simulation have been found outside Tetra Pak.



# Chapter 3

## Theory

This chapter will cover the theory used in this Thesis. This is needed to fully understand the deformation behavior and the numerical solution methods. The main topics that will be described are the basics of Corrugated boards, large deformations, Yield Criterion and the solution method for ABAQUS/Explicit.

### 3.1 Box Compression

Box compression test (BCT) is a test to measure corrugated and package boards strength, in Korin, Ristinmaa and Ottosen [13] a theoretical model is given to calculate the box compression resistance (BCR) with material properties and by dividing the package into flap and corner panels. The material properties needed is the short span compression test (SCT) and bending resistance (BR) values in the MD and CD direction. The predictions from the model deviated less than 20% from the physical BCT. The analytical prediction of the BCR were tested on Tetra Brik packages in the internal report by Muzzi and Tryding [15]. The simple model predicted the BCR accordingly to the physical test, however the model does not take geometry change into account. The correlation of a BCT and package with perforation is discussed in Innventia report [16] the conclusions was that BCR is not directly affected by perforation but the damages occurred during BCT is affected by perforation.

### 3.2 Corrugated Board

In Abaqus linear quadrilateral shell elements of type S4R is used, the elements have a multilayer capability which can model sandwich structure such as corrugated board. In a sandwich structure the different layers is assumed to be homogeneous and orthotropic. The fluting, i.e the inner layer was modeled as a homogeneous core with equivalent material properties as the physical material, see 3.1. The transition procedure is described in T. Nordstrand [17] is used.

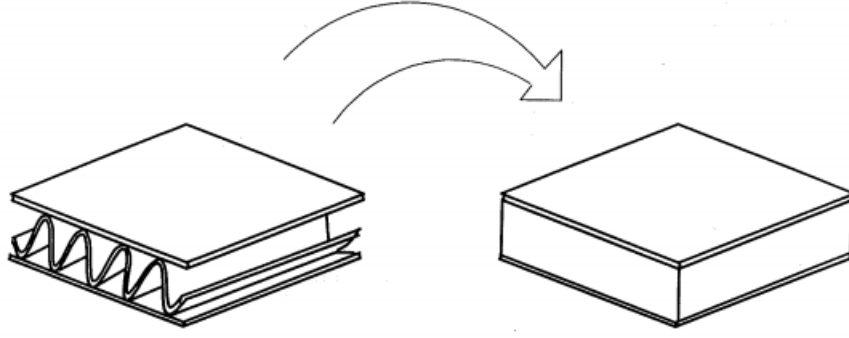


Figure 3.1: Transition of the structural core to a homogeneous core

The effective core moduli can be approximated as follows

$$E_{y,2} = \frac{\alpha S_{2,c}}{h_c} \quad (3.1)$$

where  $\alpha$  is the take-up factor,  $h_c$  is the core thickness and  $S_{2,c}$  is the tensile stiffness of the corrugated core sheet in the CD-direction.

From the known relationship between the elastic constants of an isotropic material

$$G = \frac{E}{2(1 + \nu)} \quad (3.2)$$

$E$  and  $\nu$  can be replaced with the geometric means of the in-plane elastic constants

$$G_{12} \approx \frac{(E_1 E_2)^{1/2}}{2[1 + (\nu_1 \nu_2)^{1/2}]} \quad (3.3)$$

In Baum, Brennan and Habeger [18] the geometric mean value of  $(\nu_1 \nu_2)^{1/2}$  was found to be a constant equal to 0.293, this simplifies the formula to

$$G_{12,j} \approx 0,387 \sqrt{E_{1,j} E_{2,j}} \quad (3.4)$$

where  $j$  is the composite layers 1-3. However the expression for  $G$  in equation 3.4 should only be used for papers with anisotropy ratios less than 3.

The density for the homogeneous core is calculated with

$$\rho_{core} = \alpha \rho_{fluting} \frac{t}{h_c}, \quad (3.5)$$

where  $t$  is the thickness of the fluting and  $\rho_{fluting}$  is the density of the fluting.

### 3.3 Continuum Mechanics

#### 3.3.1 Hill's Yield Criterion

Hill Yield Criteria is an anisotropic yield function used to model the paperboard in this work. The concept of an anisotropic yield function was originally developed by

Von Mises (1928) and the function can be expressed as

$$f = \boldsymbol{\sigma} : \mathbf{F} : \boldsymbol{\sigma} - 1 \quad (3.6)$$

where  $\mathbf{F}$  contains the material parameters. In the general three dimensional case the tensor  $\mathbf{F}$  has 21 parameters to be determined. However, paperboard is an orthotropic material and the number of parameters can therefor be reduced to 9 in the three dimensional case. Hill (1948) reduced the number of parameters to be determined even further by assuming that only the deviatoric stresses affects the yielding. This allowed for only 6 parameters to be included. The Hill plasticity model may be determined simply by comparing the model to the Mäkelä-Östlund model when the models are restricted to  $J_2$  -flow theory and orthotropy. The comparison is done via the effective stress of the two models. The effective stress measure for the Hill plasticity model may be expressed as

$$\sigma_e = [(G + H)\sigma_1^2 + (F + H)\sigma_2^2 + (F + G)\sigma_3^2 - 2F\sigma_2\sigma_3 - 2G\sigma_1\sigma_3 - 2H\sigma_1\sigma_2 + 2L\sigma_2^2\sigma_3 + 2M\sigma_1^2\sigma_3 + 2N\sigma_1^2\sigma_2]^{1/2}. \quad (3.7)$$

The effective stress measure of the corresponding orthotropic  $J_2$  -flow version of the Mäkelä-Östlund model is given by [7]. The result from the comparison gives that the Hill Plasticity model may be identified in terms of parameters of the Mäkelä-Östlund model as

$$\begin{aligned} G + H &= \frac{1}{3}(3a^2 + b^2 + c^2 - 2bc) \\ F + H &= \frac{1}{3}(a^2 + 3b^2 + c^2 - 2ac) \\ f + G &= \frac{1}{3}(a^2 + b^2 + 3c^2 - 2ab) \\ N &= \frac{3}{2}d^2 \\ M &= \frac{3}{2}e^2 \\ L &= \frac{3}{2}f^2. \end{aligned} \quad (3.8)$$

All parameters  $a$ ,  $b$ ,  $c$ ,  $d$ ,  $e$  and  $f$  are identified in [7] and the derivation of these will not be included in this report.

Restricting the Hill Plasticity model to transversal isotropy the parameters of the Hill plasticity model can be expressed as

$$\begin{aligned}
F &= K_{22}^{\frac{2\tilde{N}}{\tilde{N}+1}} - \frac{1}{2}, \\
G &= H = \frac{1}{2}, \\
L &= 2K_{22}^{\frac{2\tilde{N}}{\tilde{N}+1}} - \frac{1}{2} \quad \text{and} \\
N &= M = 2K_{45}^{\frac{2\tilde{N}}{\tilde{N}+1}} - \frac{1}{2}K_{22}^{\frac{2\tilde{N}}{\tilde{N}+1}}.
\end{aligned} \tag{3.9}$$

Where  $K_{22}$ ,  $K_{45}$  in equation 3.9 carries all information on the differences in plastic material behavior between the different material directions and  $\tilde{N}$  is a master value of the strain-hardening exponent.

### 3.3.2 Calibration of paperboard data to Hill plasticity model

The following section treat an analytical procedure for calibration of the Hill plasticity model in ABAQUS.

#### Elasticity

The calibration is based on tensile test data. The tensile stiffness in the MD,  $E_1$ , and tensile stiffness in CD,  $E_2$ , are from tensile test data. The determination of the tensile stiffness in ZD direction is complex to perform, either tensile or compression testing is needed. An approximation for accurate modelling of the in-plane behavior found by Mäkelä and Tryding [8] and given as

$$E_3 = 0.0068\sqrt{E_1E_2}. \tag{3.10}$$

The in-plane Poisson's ratio is evaluated by combining Baum's approximation [9] with symmetry requirement of the stiffness tensor,

$$v_{12} = 0.293\sqrt{\frac{E_1}{E_2}}. \tag{3.11}$$

Stenberg and Fellers [10] showed that paper materials can exhibit both positive and negative out-of-plane Poisson's ratios. Due to the small impact it has on the mechanical behavior a suitable approximation is to assume they are zero, i.e

$$v_{13} = v_{23} = 0. \tag{3.12}$$

In-plane shear testing of paper is highly complex because thin plates tend to buckle, instead the in-plane shear modulus is determined from tensile test in the 45 °-direction. After some manipulation the expression for in-plane shear modulus is,

$$G_{12} = \frac{1}{\frac{4}{E_{45}} + \frac{(2v_{12} - 1)}{E_1} - \frac{1}{E_2}}. \tag{3.13}$$

Because the Poisson's ratio in the out-of-plane is equal to zero the plane shear stiffness is calculated with these simple relations,

$$G_{13} = \frac{1}{2}\sqrt{E_1 E_2} \quad \text{and} \quad G_{23} = \frac{1}{2}\sqrt{E_2 E_3}. \quad (3.14)$$

### Plasticity

The plasticity, isotropic hardening and rate independent yield, requires to be defined with yield stress,  $\sigma_f$ , and plastic strain,  $\epsilon^p$ . The relation between the yield stress and plastic strain is given by

$$\epsilon^p = \left( \frac{\sigma_f}{\tilde{E}_0} \right)^{\tilde{N}}. \quad (3.15)$$

To be able to start an analysis in ABAQUS the yield stress at zero plastic strain should be defined. A suggested solution is to assume that plasticity is initiated when the plastic strain in equation 3.15 is one thousandth of the elastic strain,

$$\sigma_{f0} = \left( \frac{\tilde{E}_0^{\tilde{N}}}{1000 E_1} \right)^{\frac{1}{\tilde{N} - 1}}. \quad (3.16)$$

The plasticity data needs to be on regularised form (equidistant plastic strain values) in ABAQUS/Explicit to minimize time-consuming table lookups during simulations. The regularised form is accomplished by selecting a constant plastic strain increment,  $\Delta\epsilon^p = 0.0001$ , and the two following expressions,

$$\epsilon_i^p = \epsilon_{i-1}^p + \Delta\epsilon^p \quad \text{and} \quad (3.17)$$

$$\sigma_{f1} = \tilde{E}_0(\epsilon_i^p)^{\frac{1}{\tilde{N}}}. \quad (3.18)$$

### Anisotropy

Anisotropic plasticity according to Hill plasticity needs to be defined as yield stress ratios in different material directions, these yield stress ratios can be expressed in terms of the Hill parameters  $F$ ,  $G$ ,  $H$ ,  $L$ ,  $M$  and  $N$  as

$$R_{11} = \frac{1}{\sqrt{G + H}}, \quad (3.19)$$

$$R_{22} = \frac{1}{\sqrt{F + H}}, \quad (3.20)$$

$$R_{33} = \frac{1}{\sqrt{F + G}}, \quad (3.21)$$

$$R_{12} = \sqrt{\frac{3}{2N}}, \quad (3.22)$$

$$R_{13} = \sqrt{\frac{3}{2M}}, \quad (3.23)$$

$$R_{23} = \sqrt{\frac{3}{2L}}. \quad (3.24)$$

### 3.3.3 Kinematics of large deformations and small strains

Consider an arbitrary reference configuration where  $\mathbf{X}$  and  $\mathbf{x}$  denotes the position of a particle in the reference and deformed configuration, respectively. The relation between them is given by the deformation gradient, i.e.

$$\mathbf{F} = \frac{d\mathbf{X}}{d\mathbf{x}}. \quad (3.25)$$

Plasticity models in ABAQUS/explicit is based on a few fundamentals postulates, this means that all of the elastic-plastic response models have the same general form. Models are written either as rate-independent or rate-dependent models. A rate-independent model is one which the constitutive response does not depend on the rate of deformation, vice versa for a rate-dependent.

An assumption of elastic-plastic models is that the total deformation can be divided into two parts using, a so-called, multiplicative split between the elastic and the plastic part, i.e.

$$\mathbf{F} = \mathbf{F}^e \mathbf{F}^p, \quad (3.26)$$

where  $\mathbf{F}$  is the total deformation gradient,  $\mathbf{F}^e$  is the fully recoverable part and  $\mathbf{F}^p$  is the plastic part. See the illustration of the relation below in figure 3.2.

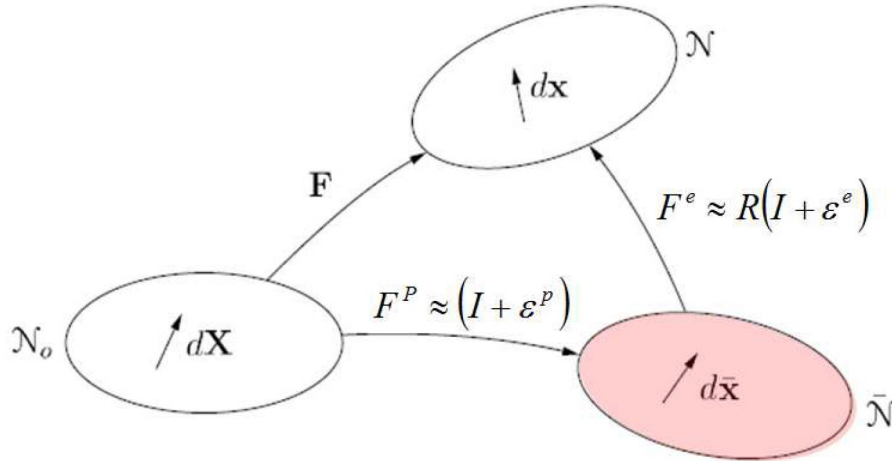


Figure 3.2: Mapping of the reference configuration to the deformed configuration for large deformations and small strains. In the figure is  $\mathcal{N}_o$ ,  $\mathcal{N}$  and  $\bar{\mathcal{N}}$  the reference, immediate and final configuration.  $R$  is the rotation matrix.

## 3.4 Finite Element Model

### 3.4.1 ABAQUS/Explicit

This method is efficient for problems with short load durations or large deformations. ABAQUS/Explicit uses the explicit central-difference integration rule to integrate the



equation of motion for a arbitrary body [12],

$$\mathbf{M}\ddot{\mathbf{u}}^{(i)} = \mathbf{f}_{ext}^{(i)} - \mathbf{f}_{int}^{(i)}, \quad (3.27)$$

where the diagonal mass matrix  $\mathbf{M}$ , the external force vector  $\mathbf{f}_{ext}$  and the internal force vector  $\mathbf{f}_{int}$  is used to calculate the nodal acceleration  $\ddot{\mathbf{u}}$ . This calculation is performed at the beginning of every increment. With the known acceleration the velocity at the next time step can be computed according to

$$\dot{\mathbf{u}}^{(i+\frac{1}{2})} = \dot{\mathbf{u}}^{(i-\frac{1}{2})} + \frac{\Delta t^{(i+1)} + \Delta t^{(i)}}{2} \ddot{\mathbf{u}}^{(i)}. \quad (3.28)$$

This obviously requires that the initial velocity,  $\dot{\mathbf{u}}^{i-\frac{1}{2}}$ , is known. Furthermore when the velocity is obtained the displacement can be calculated according to

$$\mathbf{u}^{i+1} = \mathbf{u}^{(i)} + \Delta t^{(i+1)} \dot{\mathbf{u}}^{(i+\frac{1}{2})}. \quad (3.29)$$

At the first time step where  $t = 0$  the velocity  $\dot{\mathbf{u}}(0)$  and the acceleration  $\ddot{\mathbf{u}}(0)$  is defined by the user or set to zero.  $\mathbf{u}^{(+\frac{1}{2})}$  and  $\mathbf{u}^{(-\frac{1}{2})}$  are still unknowns, these can be determined by the following equations

$$\mathbf{u}^{(+\frac{1}{2})} = \dot{\mathbf{u}}^{(0)} + \frac{\Delta t^{(1)}}{2} \ddot{\mathbf{u}}^{(0)} \quad \text{and} \quad (3.30)$$

$$\mathbf{u}^{(-\frac{1}{2})} = \dot{\mathbf{u}}^{(0)} - \frac{\Delta t^{(1)}}{2} \ddot{\mathbf{u}}^{(0)}. \quad (3.31)$$

The next step in an explicit integration scheme is to determine the strain increments followed by the stresses and internal forces. The big disadvantage when using the explicit method is that small errors are introduced at every solved equilibrium, this can make the solution unstable [19]. To avoid this phenomena one has to use a time integration that is small enough to keep the acceleration within the increment constant. ABAQUS/Explicit uses the stable time step of

$$\Delta t \leq \frac{2}{\omega_{max}} (\sqrt{1 + \xi^2} - \xi), \quad (3.32)$$

where  $\xi$  is the fraction of critical damping in the highest mode and  $\omega_{max}$  is the highest frequency of the system.

There are two strategies that are used to control the time step, either using a fixed time step or calculating a new time increment. To obtain an approximation of the stable time step the follow expression is used

$$\Delta t = \frac{L_{min}}{c_d}, \quad (3.33)$$

where  $L_{min}$  is the smallest dimension in the generated mesh and  $c_d$  is considered to be the wave speed and is expressed as

$$c_d = \sqrt{\frac{E}{\rho}}, \quad (3.34)$$

where  $E$  is the Young's modulus and  $\rho$  the mass density. One way for ABAQUS to handle time demanding iteration scheme is to use mass scaling. This function increases the mass of the part by increasing the mass density  $\rho$ . By this follows a decreased wave speed  $c_d$  and an increased  $\Delta t$ , which results in a shorter solution time.

### 3.4.2 Shell elements

When model a finite element model with a slender structure and with continuum elements, such as a package, shell elements can be used because of kinematic assumptions. The assumptions lower the number of degrees of freedom and the computational cost. The evaluation of using shell elements for modeling corners and creases is done by Magnusson, Nyman and Ristinmaa [21].

The conventional shell element S4R have a uniformly reduced integration to avoid shear and membrane locking, it converges to shear flexible theory and for thick shells and classical theory for thin shells, see figure 3.3.

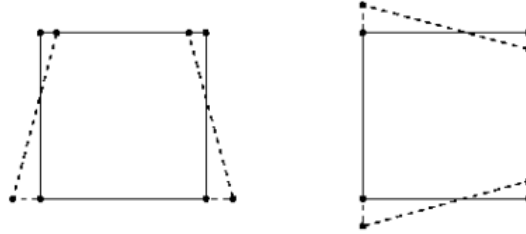


Figure 3.3: S4R elements with illustration of the hourglass modes that can propagate over the mesh.

The S4R element is used throughout this master thesis for its wide range of applications [12].

# Chapter 4

## 3D Scanner Test

### 4.1 Introduction

This chapter presents the method and result from the physical tests of a 3D scanner. The physical test was performed to gain more knowledge and investigate of how the package geometry was in reality, the chapter is therefore separated from the other test.

### 4.2 3D Scan

The perfect package, CAD model, differs from the package produced physical, this geometry change is needed to be able to model a more realistic package. With a 3D scan the exact dimension of a package can be investigated. The geometry change between packages was also of interest therefore several packages were scanned too identify recurring imperfections.

#### 4.2.1 Samples

The samples were Tetra Recart package 500 ml, the packages where left to dry for 2 hours on a carriage after sterilization. The surrounding temperature and relative humidity were 23 °C and 50% RH, respectively.

#### 4.2.2 Test Equipment

The 3D scanner used was a Atos Core 300, see figure 4.1. Each scan takes 5 minutes to perform. The 3D scanner scan the package at 5 location during a full 360° rotation. The bottom of the package was excluded in the scan. The integrated software saved the 3D images as stl.-files and the result was later imported to ABAQUS for analysis.



Figure 4.1: 3D scanner used [22].

### 4.2.3 Result

In figure 4.2 the result from one package is seen, the 3D images received are well detailed and the geometry is easily to distinguish. The geometry described below was reoccurring on all of the tested packages.

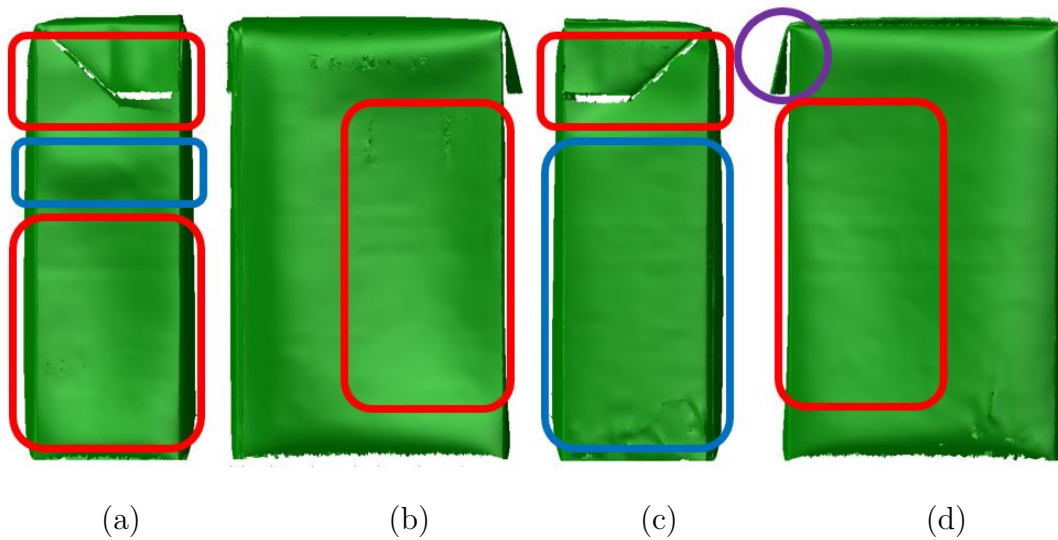


Figure 4.2: The four panels of a scanned package. The blue rectangles mark where the package are buckling outwards and the red rectangles are where the package is buckling inwards, compared to if the panels had been vertical. The purple ring marks the flap that have a distinct outward position.

The small blue rectangle in 4.2 (a) differed between packages, in half of the packages this area had a inward buckling. The back and front panel, (b) and (d), had a outward buckle in the unmarked area.

#### 4.2.4 Analysis

The geometry of a produced package differ largely to the designed one. After the sterilization the TRC package are dried on a steel rack with the longitudinal sealing and top resting downwards. The packages final geometry is received from this step, due to gravity the package is bulging alongside the panel and not in the bottom. The underlaying flap gets pressed into the side panel when the opposite flap is dried in an outward position, marked in figure 4.2 (d) with a ring.

If the package is left standing for days the gravity rearrange the geometry to more bulging in the bottom and slimmer top, still the geometry received from the drying process is visible.



# Chapter 5

## Top Load Compression Tests

### 5.1 Introduction

The test were performed at three different occasions. On the first occasion the primary package was tested. Several different set-ups where tested to gain knowledge of the package and to collect information for validation of the finite element model. Next test occasion the secondary package was tested and lastly the secondary unit was tested. The main purpose of these test was to understand the packages better, how the buckling modes behaved and at what external force the buckling was initiated. The section is divided into three sub-chapters in accordance to the performed tests. The compression tests was done according to Tetra Pak's internal test method I021.43 [25], with small deviations fully explained.

#### 5.1.1 Samples

The primary package samples were Tetra Recart package 500 ml, the packages where left to dry for 2 hours on a carriage after sterilization. The surrounding temperature and relative humidity were 23 °C and 50% RH, respectively. The secondary package samples were Tetra Recart secondary package 2x8 tray for 500 ml primary package. The surrounding temperature and relative humidity were 23 °C and 50% RH, respectively.

#### 5.1.2 Test Equipment

The compression test was done using a Zwick/Roell model Z005, see figure 5.1. The compression velocity were set at 50 mm/min and a maximum compression distance of 20 mm. The packages was placed in the same marked place centered under the Zwick. The instrument had an integrated software called TestXpert 2, were the data could be extracted to excel files.



Figure 5.1: Compression instrument used [23].

## 5.2 Primary Package

### 5.2.1 Method

There were some variance to the test method I021.43 shown in figure 5.2 (b) and (c).

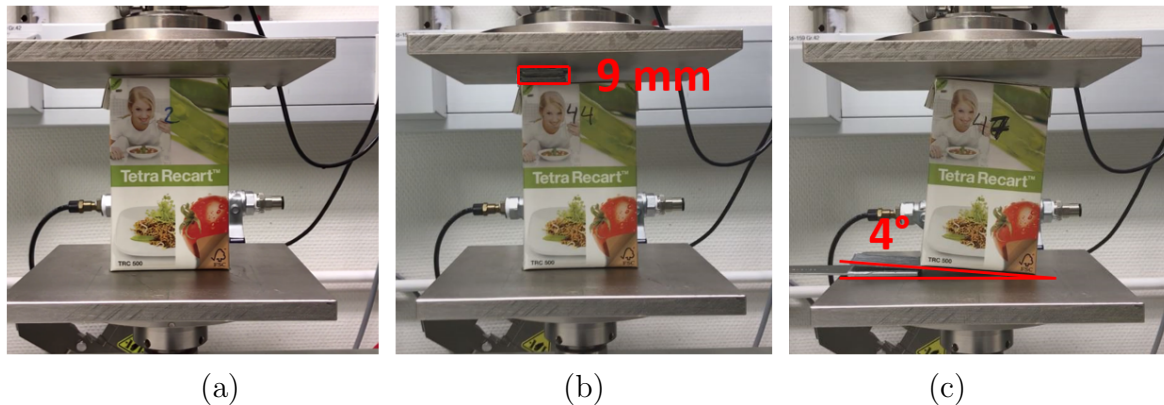


Figure 5.2: The three set-up tested; (a) Normal compression. (b) Unsymmetrical compression, where a 9 mm thick metal bar was placed above the top left corner of the package. (c) Angled compression, where the package was tilted  $4^\circ$  in the bottom

Additional normal compression was also done for Empty packages, i.e. the product liquid within the package was emptied through a small hole in the bottom and another one for packages with open flaps, i.e. there was no affection of the flaps on the package panels.

### 5.2.2 Result

#### Normal compression

Two different buckling modes is identified. In figure 5.3 the two modes is marked and can easily be distinguish from the maximum force applied before buckling. Buckling



mode 1 & 2 are presented, if the top load is higher or lower than approximately 200 N, respectively.

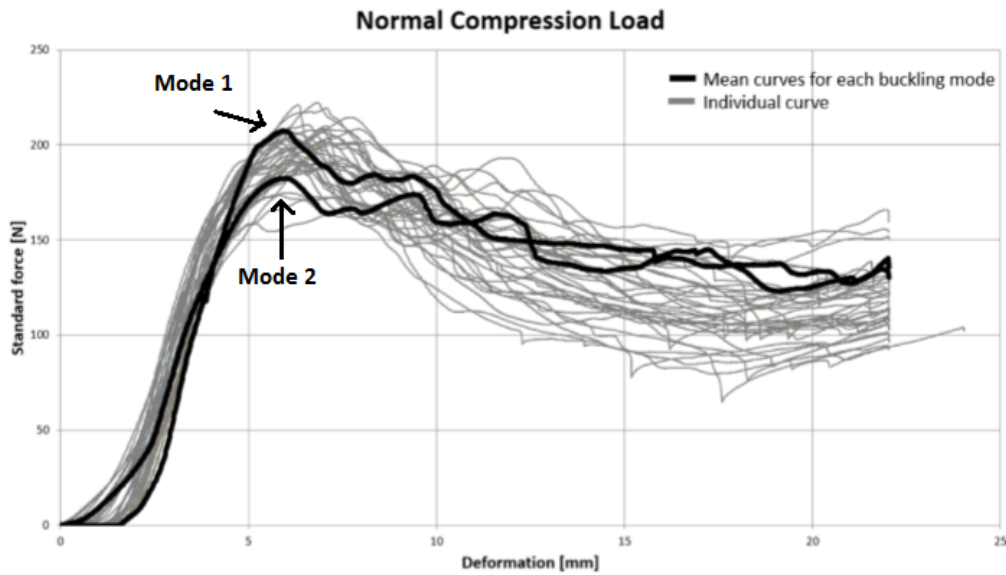


Figure 5.3: Buckling mode 1 has a top load force over 200 N and the buckling mode 2 has a top load of approximately 180 N.

Statistical analysis of the top load force data gave a p-value of 0.438 which is larger than a significant level of 0.05. Therefore the conclusion is that the data can follow a normal distribution with a mean value of 197.5 N and a standard deviation of 13.69, see figure 5.4.

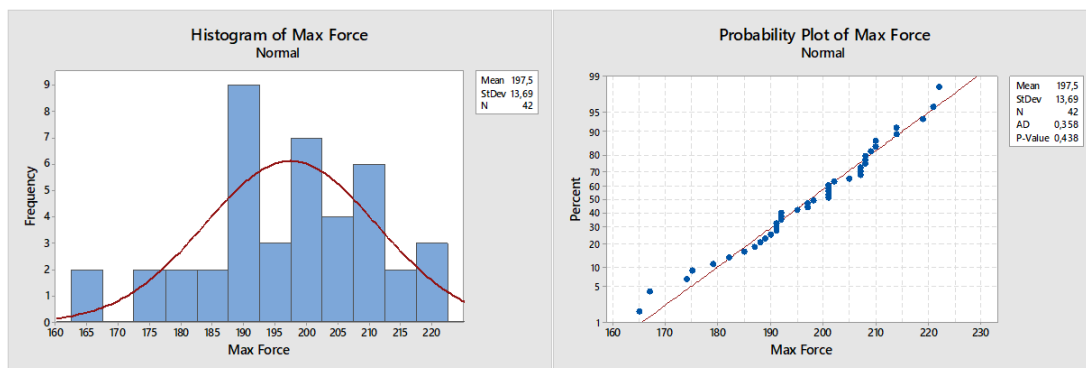


Figure 5.4: Histogram of the max top load forces registered. The data follows a normal distribution.

With a 95% normality rule the max top load force is between 170-225 N a variation of 55N [24].

### Buckling Mode 1

Mode 1 is distinguish with a distinct buckling mode in the bottom. The buckling presses both side panels inwards and the front and back panels outwards. The top half of the package show no indication of impact except for a small inclination of the top, see figure 5.5 for explanation. The propagation of the buckling is at all four corners continuously.



Figure 5.5: Illustrates the buckling behavior of Mode 1

### Buckling Mode 2

Mode 2 is initiated just below the flaps at an external load at approximately 180N. Typical the side panels are buckling opposite of each other and the same goes for the front and back panels, see figure 5.6 for a visualization. Mode 2 seems to be highly dependent of how the flaps are attached. The propagation of the buckling is at all four corners continuously.



Figure 5.6: Illustrates the buckling behavior of Mode 2

From figure 5.3 five packages with buckling mode 1 and 2 was extracted too easier distinguish them. Buckling mode 1 can be seen in figure 5.7 and buckling mode 2 can be seen in figure 5.8.

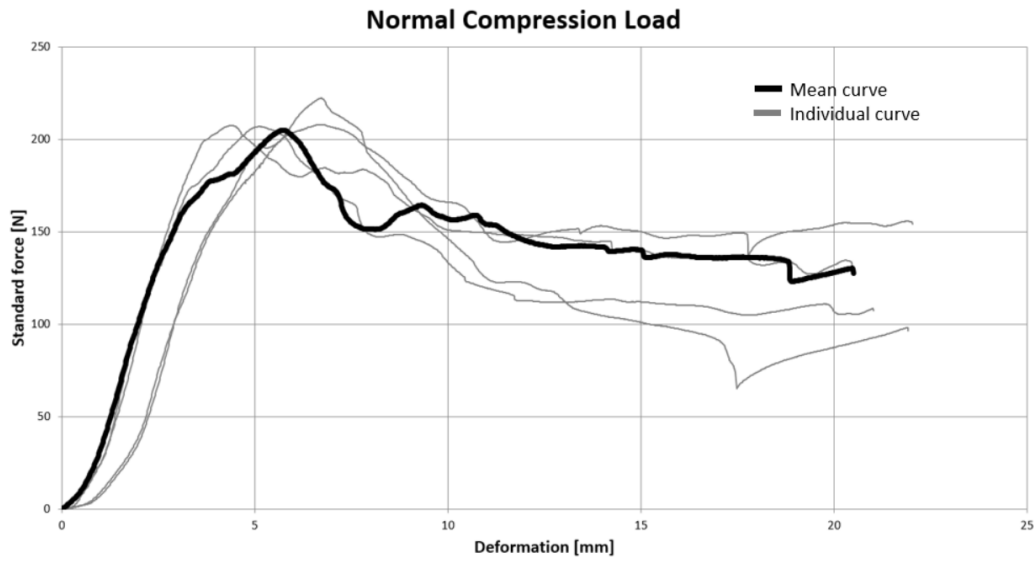


Figure 5.7: Buckling mode 1 and a BCR above 200 N.

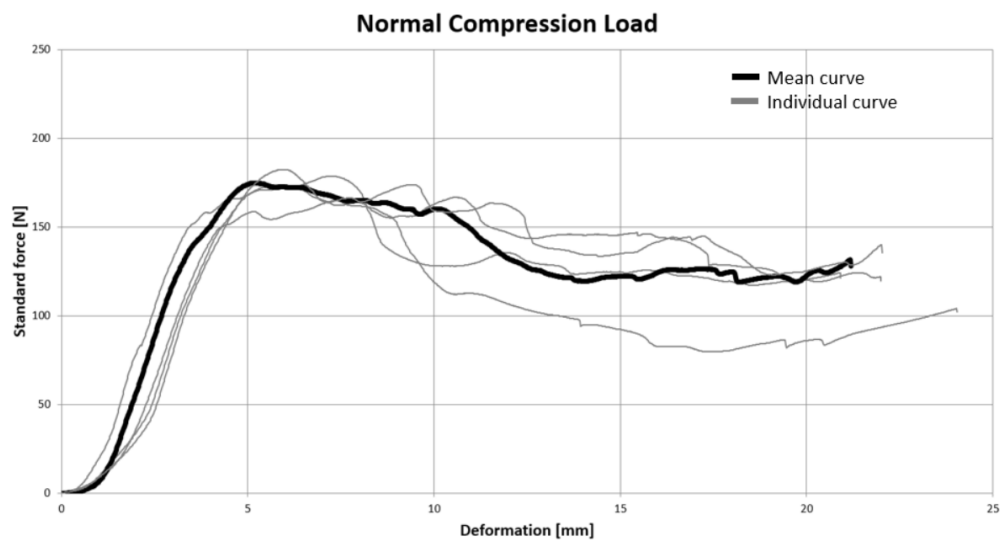


Figure 5.8: Buckling mode 2 with a BCR below 200 N, approximated around 180N.

### Unsymmetrical compression

Half of the package is compressed and buckled (peak 1), after a short period when the other half of the package meet the compression plate the force is increased again until both sides have buckled (peak 2), see figure 5.9.

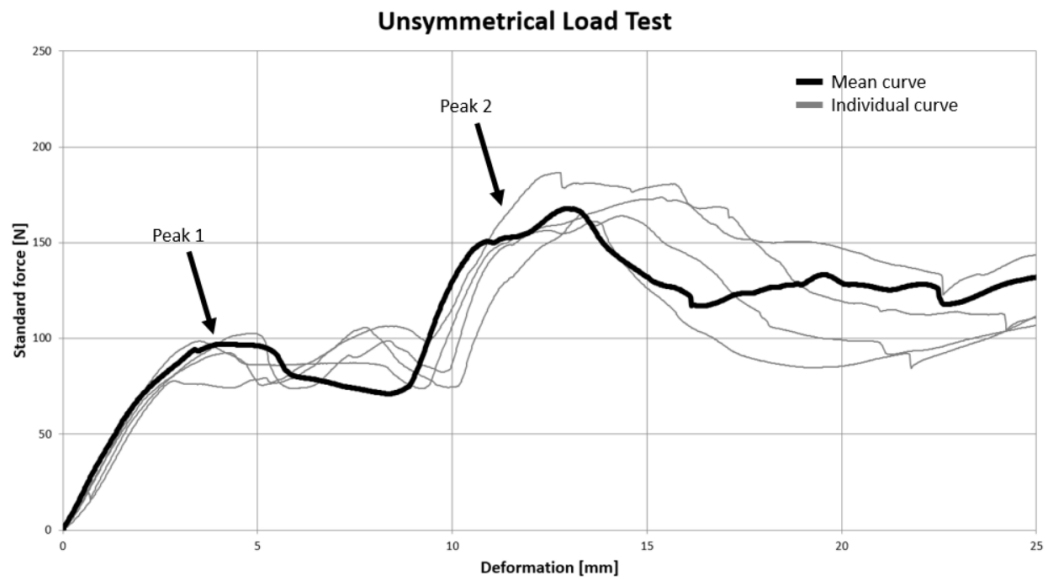


Figure 5.9: With an unsymmetrical load the package gets two compression force peaks, the two peaks represent the buckling at the different side panels.

### Angled compression

The package is first compressed at one side, when the compression plate hits the other side the whole package gets compressed this can be seen in the graph, figure 5.10, as a small bump followed by a steeper increase in load.

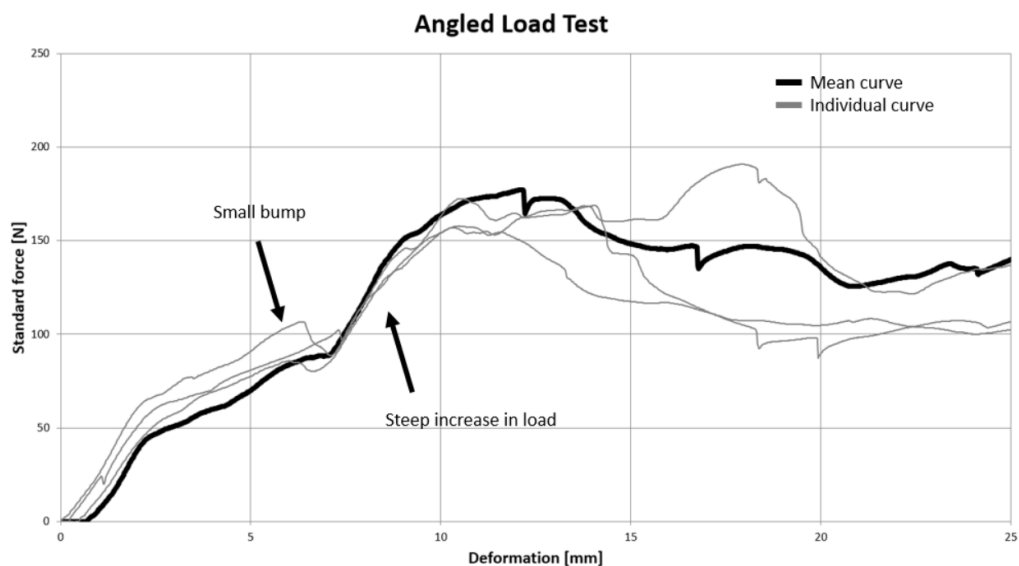


Figure 5.10: One sample shows a clear buckling peak at 6 mm deformation, the other packages shows first a buckling was initiated after contact is made with the other side, hence no real peak between 5 - 7 mm deformation.

### Empty packages

The behavior of the buckling behavior and force-displacement curves in figure 5.11 are similar to the normal compression in figure 5.7.

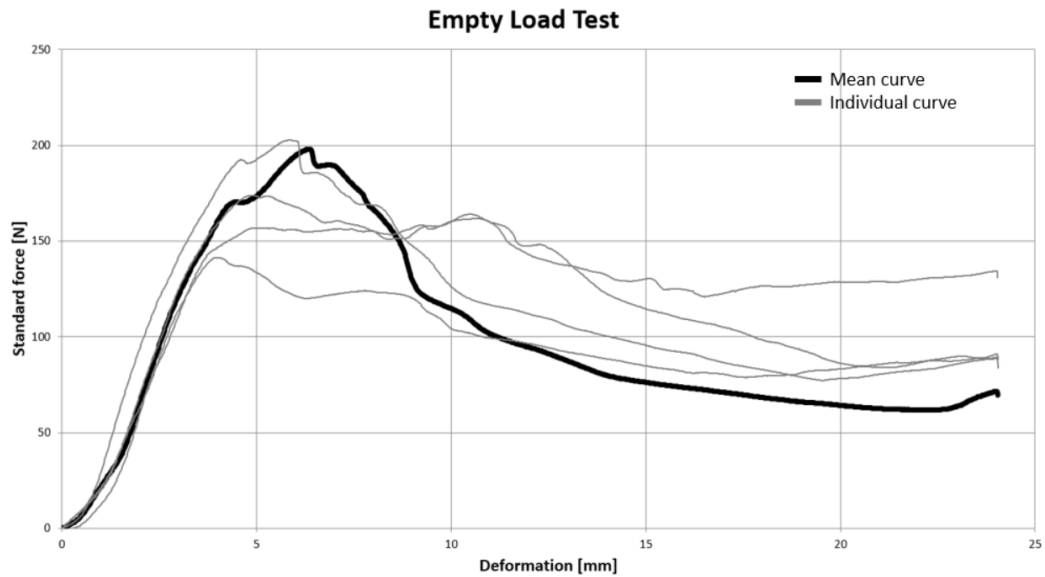


Figure 5.11: After buckling the force is continuously decreased when there is no liquid present.

### Open flaps

There is no distinct buckle in the graph, see figure 5.12, the packages are compressed with a uniform force.

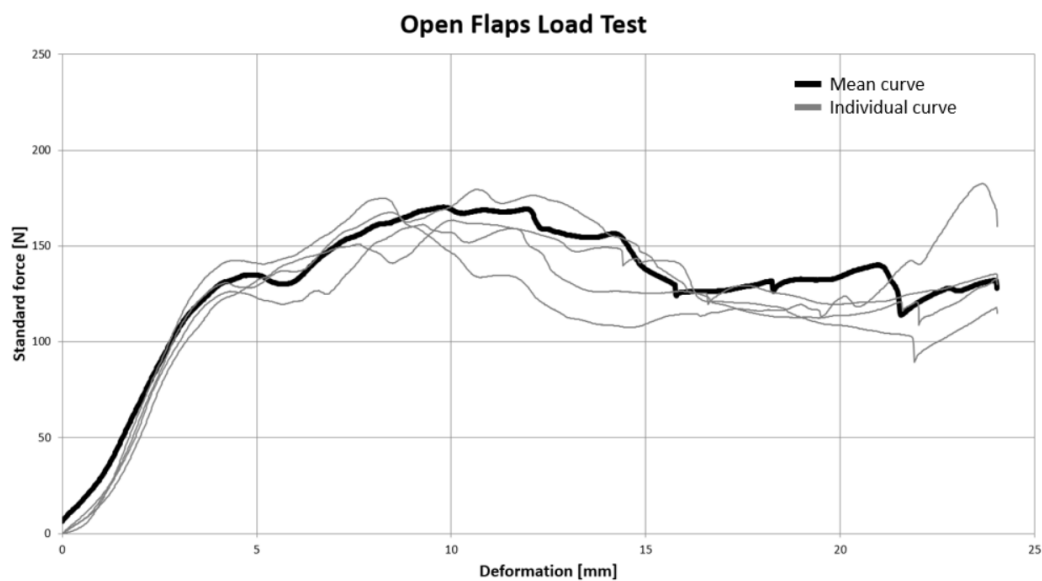


Figure 5.12: None of the packages have a BCR above 200 N in the graph.

### 5.2.3 Analysis

#### Normal

The buckling modes are highly related to the package geometry and the attachment of the flaps. The large variety in the BCR indicates how sensitive the package is for compression. In figures 5.7 and 5.8 the two buckling modes are presented in two different force- displacement graphs. Packages with buckling mode 1 is stiffer and the BCR is higher. Local buckling of the structure can be observed on some packages, this phenomena flattens out the curve. The local collapse shifts the position where the buckling initiate and the variety is large between the packages. After the buckling the compression force drops until the product inside is starting to compress.

Packages with buckling mode 2 have a different behavior. They are in general less stiff, the buckling appears at the same displacement and there is no significant force drop after buckling.

The height of the packages is unequal therefore the force-displacement curve needs to be normalized to the same point where the packages starts to compress. The curves are shifted to start the measurement at the same height.

#### Unsymmetrical & Angled

Both these result shows a similar behavior, the left side is compressed and buckled before the other side makes contact with the top plate. A difference between them is how long it takes for the second side to make contact with the compression plate.

#### Empty

The BCR are not affected if the package contains product liquid or not, what the product liquid does affect is how the compression behaves after buckling. This proves that the BCR is mainly dependent on the exact geometry of each individual package. The compression force increases when the liquid is compressed post-buckling.

#### Open flaps

None of the packages have a BCR above 200 N, the stability of the package is highly dependent on the flaps. After the first peak the force is uniform during the compression. The graph shows the same behavior as the packages with a buckling mode 2 indicating the influence of the flaps.

## 5.3 Secondary Package

### 5.3.1 Method

The same instrument was used as in previous chapter, the only difference was the compression plates were changed to a suitable size, see figure 5.13.

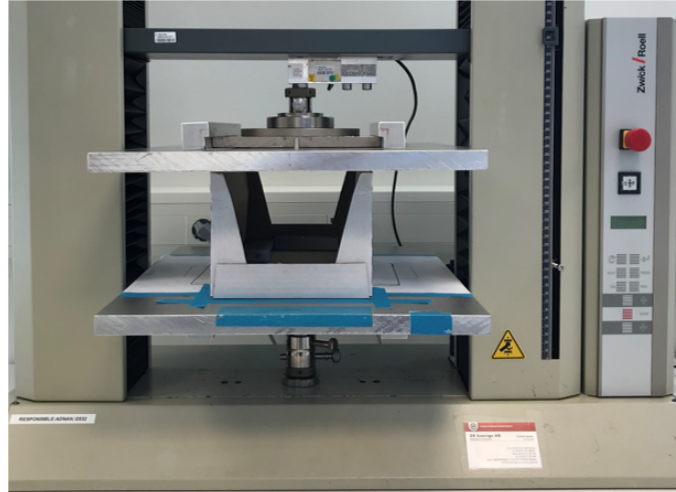


Figure 5.13: The set-up for the secondary package, the bottom of the secondary package were fixed to the bottom plate with weights.

### 5.3.2 Result

All the secondary packages showed the same buckling mode, in some top corners there was small compression of the package otherwise the only failure was buckling. All the flaps were still attached, see figure 5.14 for the force displacement graph.

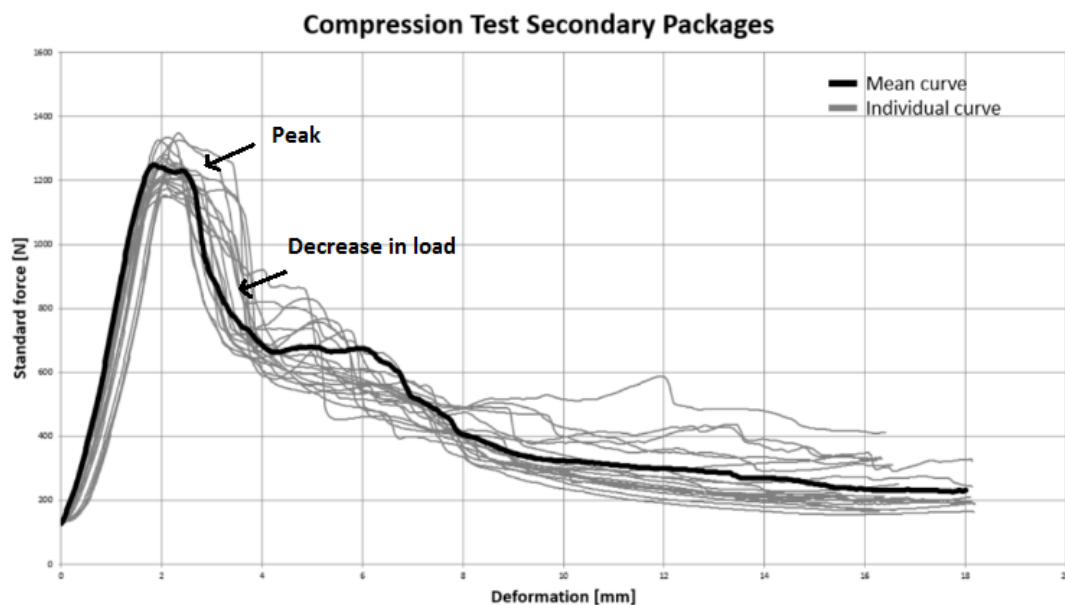


Figure 5.14: The measured force compared to the displacement in mm.

Statistical analysis of the top load force data, gave a p-value of 0.247 which is larger than a significant level of 0.05. Therefore the conclusion is that the data can

follow a normal distribution with a mean value of 1241 N and a standard deviation of 60 N, see figure 5.15.

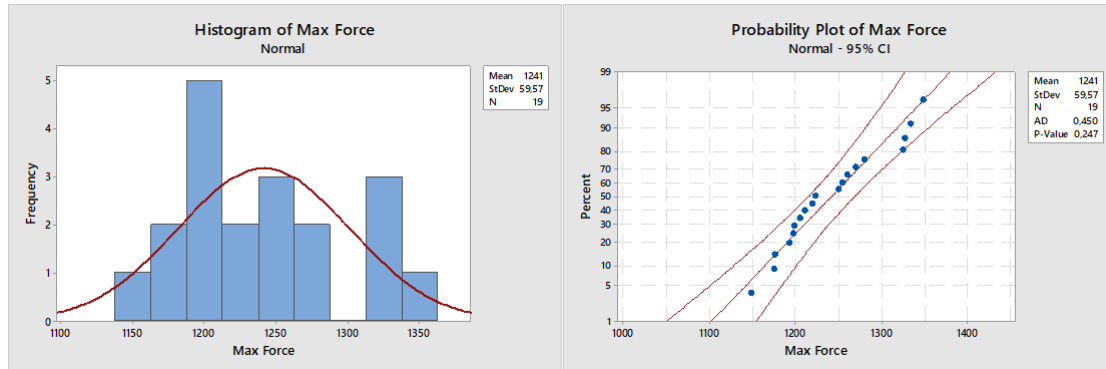


Figure 5.15: Histogram of the max top load forces registered. The data follows a normal distribution.

With a 95% normality rule the max top load force is between 1121-1361 N a variation of 240N.

In figure 5.16 the buckling mode is presented. In figure 5.16 (a) and (c) the arrow indicates where the buckling took place, on all packages the buckling started in the corner at a perforation, the buckling had a halfmoon shape and ended at a perforation on the back corner. At which perforation the buckle started varied, the top three perforations were all initiating buckles. The black ring in figure 5.16 (b) and (c) marks where local collapse appeared before the buckle. In figure 5.16 (b) both panels are buckling inwards compared to 5.16 (c) where one panel buckles outward.

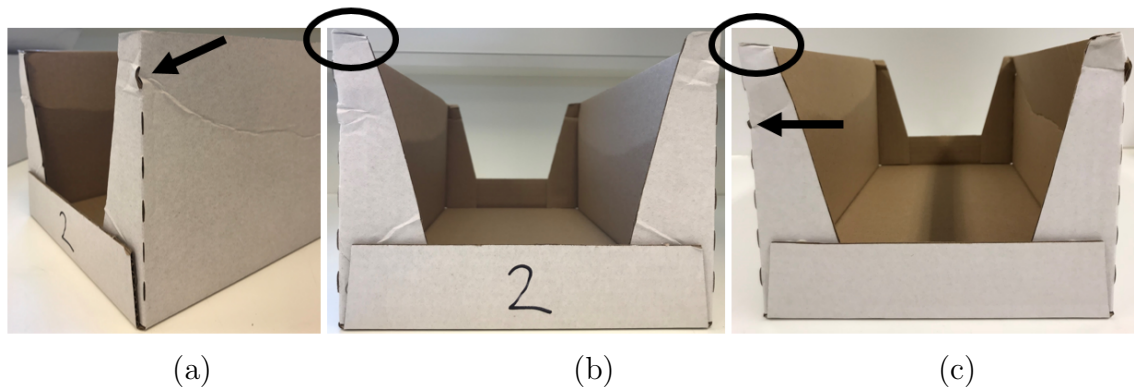


Figure 5.16: The buckling mode from the compression test.

### 5.3.3 Analysis

19 samples were tested, they all have the same incline of the curve in the beginning, the result is only shifted because the variety in the package height. After the buckling the compression force drops due to slip between the packages top edges and the



compression plate.

## 5.4 Secondary Unit

### 5.4.1 Method

A compression instrument, Zwick/Roell model Z005 [23], and a large plate for box compression was used. Due to the instrument maximum force limit of 5kN a complete compression of a secondary unit could not be performed. The maximum force was exceeded with only a small affect on the secondary package and some of the primary packages. Instead, to capture the defects emerged during transportation and to receive result that could be evaluated with a model in Abaqus, the compression was narrowed down to only compress one of the long sides, see the set-up in figure 5.17. A metal bar was attached to the upper compression plate. The bar covered the edge of the secondary package and a third of the primary package top, a width and height of 40 and 11 mm, respectively.

### 5.4.2 Result

The secondary package buckled outward similar to the previous results, it also cracked at the corner along the perforations.

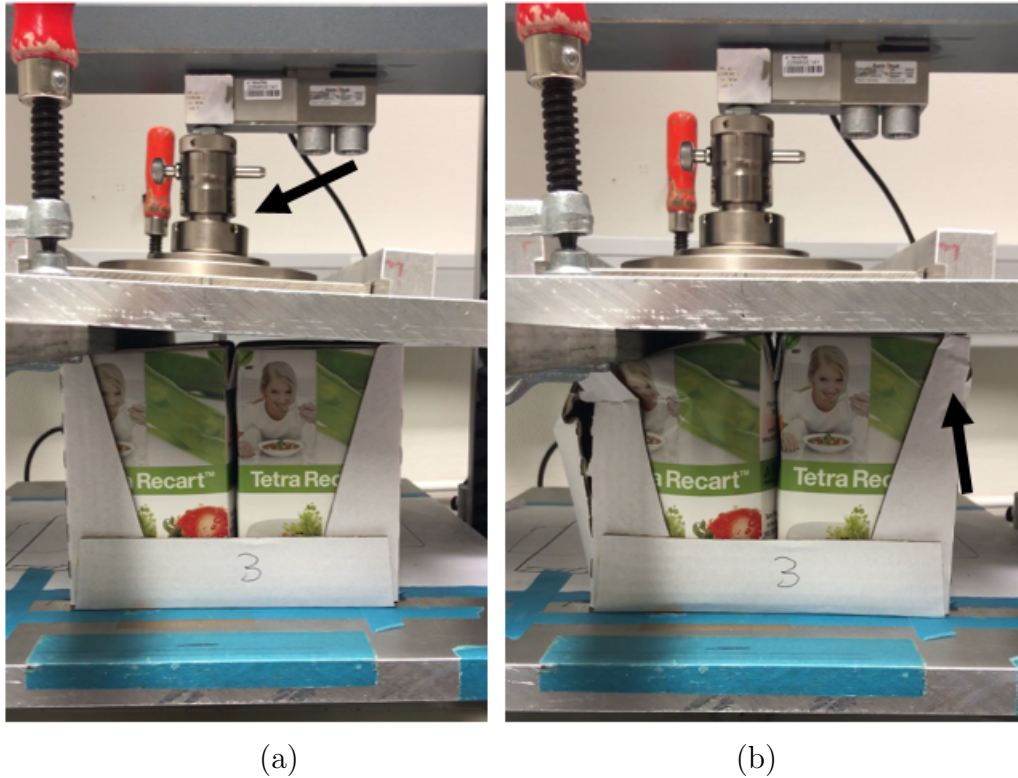


Figure 5.17: The top compression plate is attached to the Zwick instrument with a ball bearing, see black arrow picture (a), therefore the plate is tilted at the beginning and still tilted when buckling was initiated. The plate rotated to a horizontal plane post-buckling. Because of this the right side of the secondary package is compressed, see the black arrow in picture (b).

The instrument ended the compression when the maximum force was reached, the peak seen at a displacement of approximately 4 mm in figure 5.18 is the buckling of the secondary unit. The three test were normalized at 800 N because the curves started to show the same behaviour. There was a lot of data noise before 800N that did not add any valuable information.

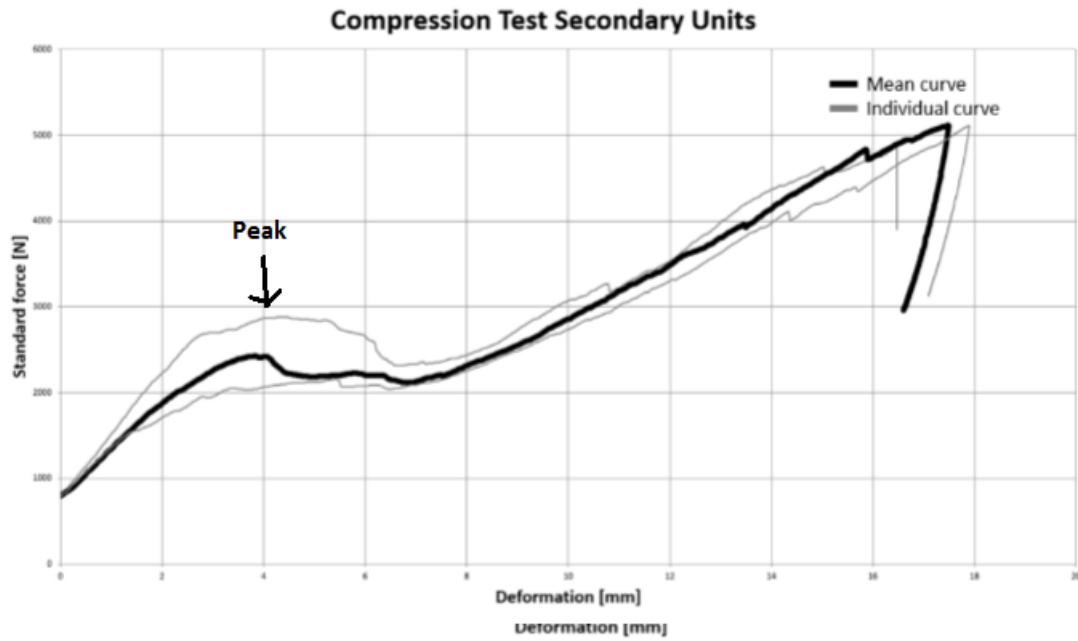


Figure 5.18: Force- displacement graph, at 5000N the instrument stop the measurement.



(a)



(b)

Figure 5.19: In picture (a) the cracked crease is visible also how all the packages have been tilted from the compression. The primary packages on the right side in the secondary package is unaffected of the compression. The secondary package have some compression on the right edge. In picture (b) the edge of the metal-bar is marked with a black line.

The primary packages buckled all in the top underneath the flaps similar to the unsymmetrical load test.

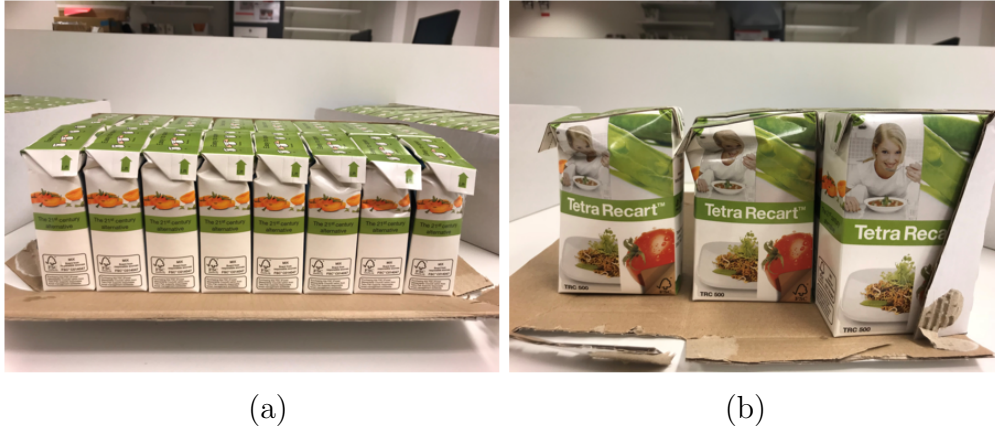


Figure 5.20: In picture (a) the buckling can easily be distinguish underneath the flaps. In picture (b) the buckling mode can be seen, each package triggered the two surrounding packages making them buckle in a similar way.

### 5.4.3 Analysis

To enable an easy comparison the results was normalized at 800N because the results where all different at first due to the allowed tilting of the plate. Hence all measured data before 800N was erased and the displacement was set to zero at 800N, the curve was left-shifted. 800 N were picked because the plate did not move and maintained the same angle until post-buckling. The buckling behavior, with an unsymmetrical load, of the secondary unit appears at a force above 2000 N. This could be compared to the normal compression test of an empty secondary package which buckles at 1200 N. The sixteen primary packages clearly supports the buckling of the secondary package, this allows an external load of more than 2000N before buckling.

The buckling of the packages happens at the same time or directly afterwards. There is a small peak and even the force-displacement curve is horizontal during this occurrence. After the buckling the cavity is compressed and the force is increased until the maximum load the machine can produce before failure.

# Chapter 6

## Finite Element Modeling in ABAQUS

### 6.1 Introduction

The FE-simulations will be performed to investigate the possibility to imitate the real behavior of a package during physical testing. The difficulties with the analysis is to obtain an exact resemblance in the geometry and correct material parameters. The FE-simulations will be performed using a computer software called ABAQUS/CAE. CAE is a pre-processor, stands for Complete ABAQUS Environment and is a graphical environment where models can be created. The pre-processor is divided into nine different modules called Part, Property, Assembly, Step, Interaction, Load, Mesh, Job and Visualization. In this chapter explanations of how the model is constructed is presented. The chapter consist of three main parts, primary package, secondary package and secondary unit. Each chapter have subsection with assumptions and limitations about the finite element models.

#### 6.1.1 Material

The material used in the simulations is provided by Tetra Pak from the internal document Testing & Calibration of Tetra Recart [26]. In the document Tetra Recart material is testing with compression and tensile test with both creased and uncreased material. Three material specimens is used in this master thesis defined as MD creases (longitudinal creases), CD creases (transversal creases) and MD CD (unfolded material). The material data used was calibrated for a temperature and relative humidity of 23 °C and 50%, respectively . The machine direction is different from other packages at Tetra Pak and can be seen in figure 6.1.

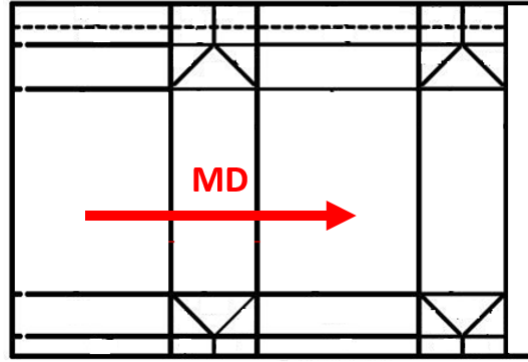


Figure 6.1: A Tetra Recart package blank where the machine direction is illustrated.

## 6.2 Geometry Dependent Rectangle

From the physical test a simple model with a changeable geometry was modeled in ABAQUS/Explicit. The model consisted of five wire sections that were lofted together, see figure 6.2. The wire sections had four different parameters to determine the geometry. Each wire were constructed to fit a cut in one of the 3D scanned package. The whole package was a shell model including the flaps and the elements used was S4R. To model the multiple layers of material and the folding at the top and bottom, the model had a variety in thickness at these different sections.

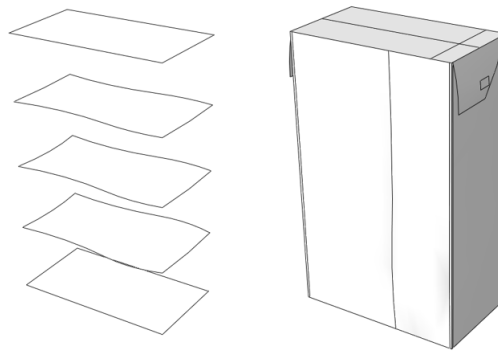


Figure 6.2: Illustrates how the simple geometry was modeled

### 6.2.1 Result

#### Assumptions

- The top and bottom wire section had a perfect rectangular geometry.
- The flaps were modeled with an arbitrary bend to capture the physical behavior.
- The creases were modeled as corners with a change in material data

The result from the compression analysis of the package together with experimental data is shown in figure 6.3.

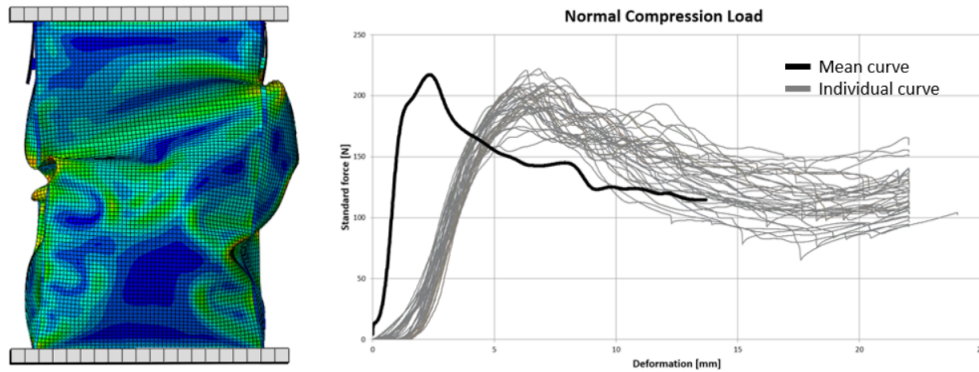


Figure 6.3: On the left the deformed package, on the right is the force-deformation curve (black line). In the background of the graph the physical test is seen.

### Limitations

- Abaqus does not have a simple way to calculate the volume of a model and with the changeable geometry trimmed by hand the volume is not controlled.
- The thickness variation does not take into consideration that folded material have several material orientations with different tensile and compression strength. The interaction between the layers are also not taken into consideration.
- Altering the geometry by hand took unnecessary time and due to user limitation in Abaqus software a more easier procedure could not be identified.

### 6.2.2 Analysis

Buckling mode 2 seems to be captured in this model with a buckling starting underneath the flap. The force-displacement curve seems to behave similarly as the physical test, with just a slightly higher BCR.

The obtained results showed to be promising, but the assumptions and limitations of the model is too large. Since Tetra Pak needs a repeatable and controllable procedure for other packages a more complex model needs to be evaluated. The steeper curve in the top load compression graph for the model compared to the physical test is because the package have straight corners, imperfections to the corners should lower the stiffness of the package to more resemblance the physical tests. To create a model with imperfections and no geometrically straight corners a folding procedure of a package was implemented.



## 6.3 Folded TRC Package

To maintain a constant volume and be able to change the geometry in a simple and realistic way a package was folded from a package sheet in ABAQUS/Explicit. The folding consisted of three different steps, rising, folding sides and folding flaps. The folding in the model is simplified to speed up the computational time and illustrates more of how a package is folded by hand than in a machine. Due to the complexity and the limited of time the element size varied along the package with bigger elements at the top and bottom including the flaps. Smaller elements could be applied to the sleeve. The folded package was then imported to a new model where the package was evaluated under simple compression.

### 6.3.1 Mesh

Two different mesh was evaluated one coarse and one fine mesh. The two meshes had the same mesh in top and bottom section due too contact problems in the folding.

#### Coarse

The coarse mesh consisted of 5177 elements in total, 5009 of these were linear quadrilateral elements of type S4R, 39 of theses were linear triangular elements of type S3 and the rest were linear triangular elements of type SFM3D3. The S3 elements where located in the folding area seen in figure 6.4. The SFM3D3 elements were used to contain the cavity inside the package during folding.

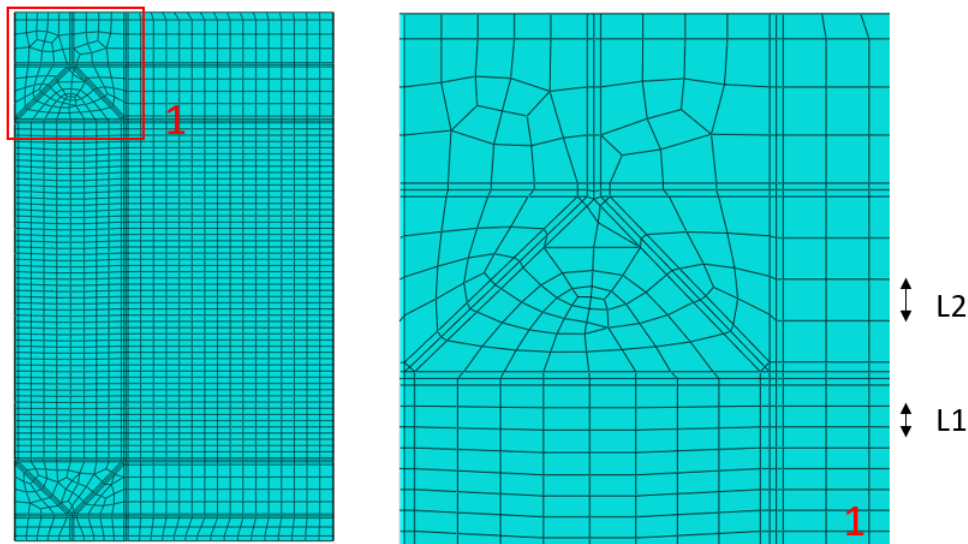


Figure 6.4: The approximate element size  $L1=2.5$  mm and  $L2=5$  mm, some of the triangular S3 elements can be seen in the right picture.



### Fine

The fine mesh consisted of 10118 elements in total. The only difference from the coarse mesh was the amount of linear quadrilateral elements of type S4R that increased to 9950 elements, see figure 6.5.

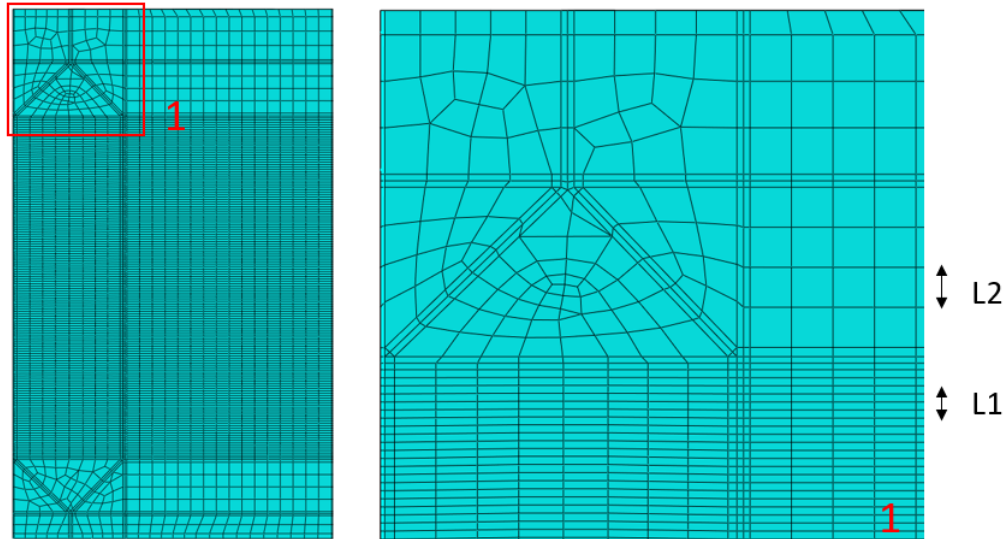


Figure 6.5: The approximate element size  $L1=1$  mm and  $L2=5$  mm, some of the triangular S3 elements can be seen in the right picture.

### 6.3.2 The folding procedure

Four inner plates were introduced at each side to rotate up the blank to form a 3D geometry. Next step was folding top and bottom using two thin plates. First the bottom and top were pressed together and then folded together. An inseparable contact was introduced to the top and bottom sealing in the beginning of the step. The folding of the flaps were done using four so called squeezers. This was a sensitive step and to avoid penetration and unnecessary contact points the squeezers had to be carefully modeled to make the step as gentle as possible. Below is the whole procedure illustrated in figure 6.6.

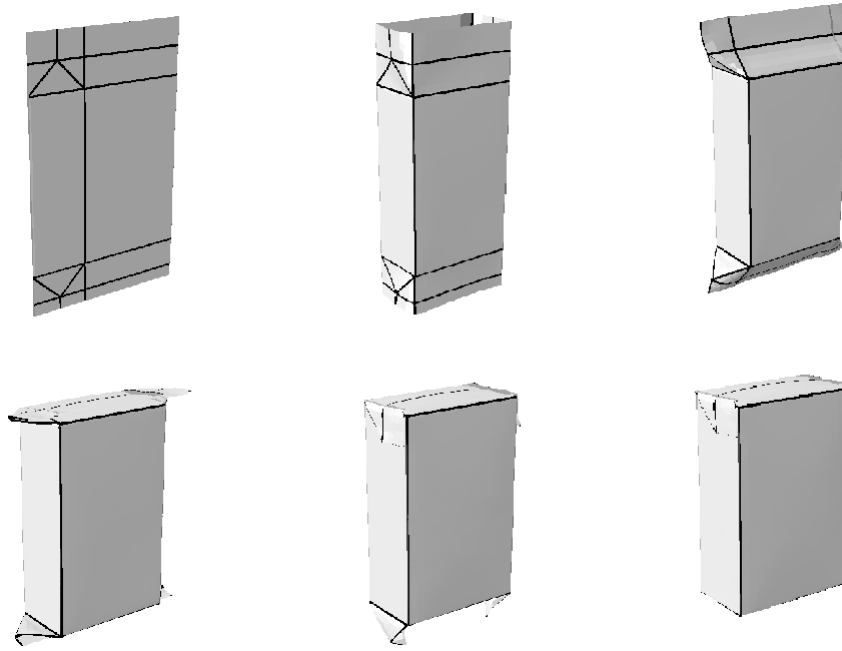


Figure 6.6: Illustration of the folding procedure, step by step from a package blank to a folded package.

### 6.3.3 Result

#### Assumptions

- The stresses and strains in the top, bottom and flaps are less important to simulate compression, therefore bigger mesh elements could be used.
- In the top and bottom sealing the model contact was smaller compared to reality for minimization of contact problems.

The result from the folding was a package with a realistic geometry where the model capture the different foldings and material intersections. The erected package is seen in figure 6.6.

Both meshes were evaluated in a Top load analysis. The differences in the force-displacement graph between a coarse and a fine mesh were negligible. The finer mesh was chosen to continue with because the details of the buckling behavior was more accurate.

#### Limitations

- The folding is sensitive, no variation of material, mesh and cavity could be done.
- The imported predefined field did not work in the compression model due to excessive element rotations.

### 6.3.4 Analysis

A more gentle folding and better defined contact should make the model less sensitive. In the compression model the material orientation, stresses and strains received from the folding could be imported as a predefined field. This however did not work properly due to wrong material definition and excessive element rotations. The sensitivity of the folding model limited the ability to solve these errors.

The ratio of the length-width of an element in a mesh is ideally one. The finer mesh had a ratio of five which can result in interpolation error. This was neglected since the model still managed to capture a realistic behavior.

## 6.4 Modified Geometry

The physical tests showed two different buckling modes that were highly dependent on the exact geometry. To find these deformation patterns in the simulations the folded TRC package's had to be slightly modified. The packages are all unique but with some resemblances, these were identified in figure 4.2 in Chapter 4.2.2.

The first one was where both flaps had been glued to the panel. This is caused during manufacturing and was not considered in the folding simulation. The other one is on the front and back panels where it buckles inwards. This deviation is caused by the hydrostatic pressure and during the cooling of the liquid inside. The package is closed with a warm liquid and later cooled, this results in a lower pressure than outside.

### 6.4.1 Modifications

To obtain a resemblance in the geometry the first step was to reduce the volume within the package. From folding the volume obtained measured at 577 cm<sup>3</sup> (577 ml). This was reduced by the interaction property Fluid Exchange defined as Mass flux and from a cavity to the environment. During the same process as the fluid exchange the wanted geometry was also obtained through a setup that kept the structure of the package. The panels at the short sides of the package were set to be shorter to allow both flaps to be pushed in as seen from the scanned packages in figure 4.2. An illustration of how the setup was done is shown in figure 6.7.

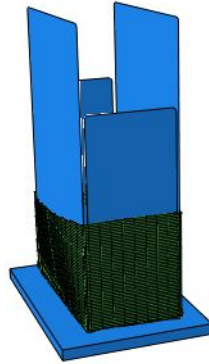


Figure 6.7: An illustration of how the geometry was maintained during the Fluid Exchange. The package is cut in half to easier present the plates that preserved the geometry. The inner plates at the side panels are shorter to allow the flaps to be pressed inwards.

To reduce the volume by more than 10%, from 577 to 500 cm<sup>3</sup> and simultaneously maintain a proper geometry configuration is a difficult task. Several tries were done with different results, but a geometry with a volume of 500 cm<sup>3</sup> was never obtained. The model with a satisfactory geometry had a volume of 514 cm<sup>3</sup>, (514 ml).

## 6.5 Final TRC Model

The final model received from the geometry change was imported to the compression model for evaluation.

### Material

In figure 6.8 the assigned material is presented to each section. The package is divided into 4 different sections. CD section is the creases presented in the top and bottom. MD section is the the longitudinal creases along the sides. LS section is where the package blank is glued together, the section has a double material thickness and is constructed with both MDCD material and CD creases material, see figure 6.8(c) Board section is all the panels around the package and the top and bottom, i.e. the material that is left unmarked in figure 6.8.

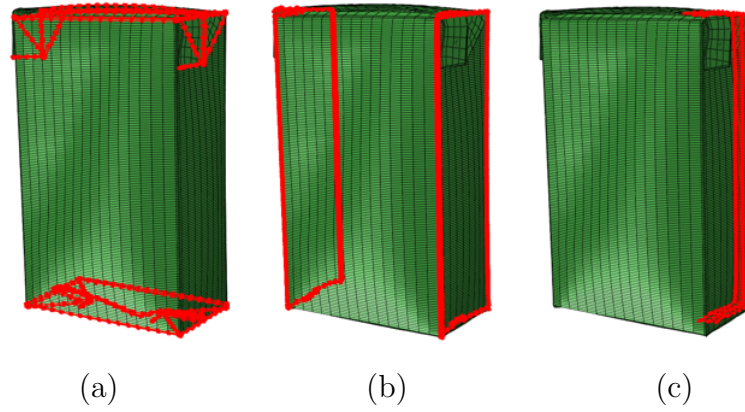


Figure 6.8: In (a) the CD section with CD creases material, (b) the MD section with MD creases material and in (c) the LS section with both MD and CD creases material.

### Tie Constraints

On the TRC package the bottom and top sealing is constrained together with induction, melting the polymer layer together. The bottom and top flaps are instead constrained together by heating the polymer layers. To imitate these constraints in the model, tie constraints are added in these sections. The tie constraints are defined with a master and slave surface and is a suitable constraint for surfaces with unmatched element nodes. The tie constraints are illustrated in figure 6.9.

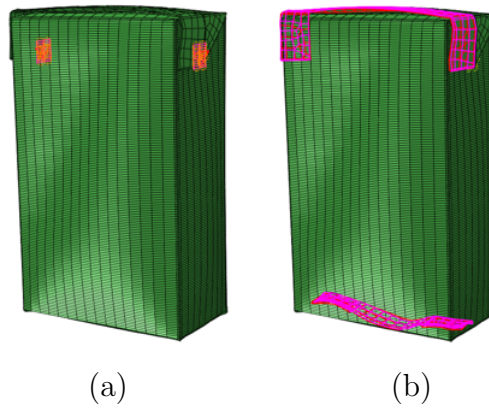


Figure 6.9: The flap constraints are seen as orange meshes in picture (a) and the top and bottom constraints are seen as pink meshes in the picture (b).

### Cavity

To model a fluid within the package a cavity was designed. The cavity consisted of both water and air to resemble the reality. A bulk modulus was calculated for the cavity. The bulk modulus was calculated with different headspace with the following

formula

$$K_{Cavity} = \frac{1}{\frac{V_{Headspace}}{V_{Package}} K_{Air} \frac{V_{Water}}{V_{Package}} K_{Water}} \quad (6.1)$$

The bulk modulus for water  $K_{Water}$  and air  $K_{Air}$  were taken at room temperature, the calculation can be reviewed in Appendix A.1.

### Hydrostatic Pressure

A hydrostatic pressure was applied to the model with the following equation

$$P = \rho gh. \quad (6.2)$$

Where the height of the package started in the top and the pressure increased from top to bottom. The density was set to be water  $\rho = 1000 \text{ kg/m}^3$  and gravity to  $g = 9.81 \text{ m/s}^2$ . The pressure applied can be seen in figure 6.10 (a).

### Underpressure

The product filled in the package holds a temperature of 50 °C the air in the headspace holds therefore the same temperature, when the package is cooled down to room temperature of 20 °C the volume minimize making a underpressure. This pressure was applied to the model and calculated with the Ideal gas law,

$$PV = nRT. \quad (6.3)$$

Where P is the pressure, V the volume of air, n is the amount of substances, R the ideal gas constant and T the temperature.

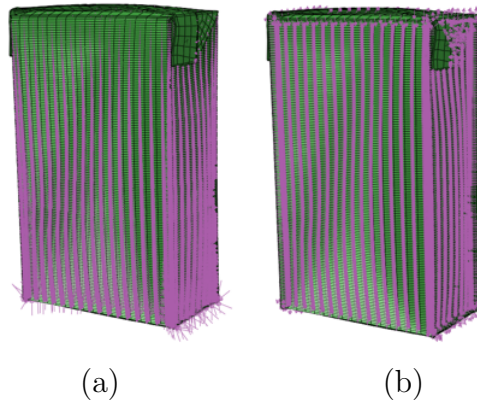


Figure 6.10: The hydrostatic pressure (pink arrows) in (a) and the under pressure (pink arrows) in (b).

## 6.6 Secondary package

### 6.6.1 Introduction

The procedure for the secondary package finite element model was similar to the primary package. First a model was design according to the drawing, then several improvements where made to the model to resemblance the physical tests. All the improvements are described in this chapter.

#### Modification to Drawing

A secondary package is never perfect in reality. One parameter that differs between packages is the angle of the panels. This should obviously be  $90^\circ$  but can easily vary depending on the variation of the machine. To capture this occurrence a  $1^\circ$  was added to the angle, see figure 6.11 (a) for an explanation.

#### Imperfections

It exist more imperfection to a package but harder to detect without doing an 3D scan, to capture these imperfections existing on the panels or in the material a buckling analysis was done. Four of the modes in the analysis was introduced as imperfections and imported to the compression model, in figure 6.11 (b) the four buckling modes is presented.

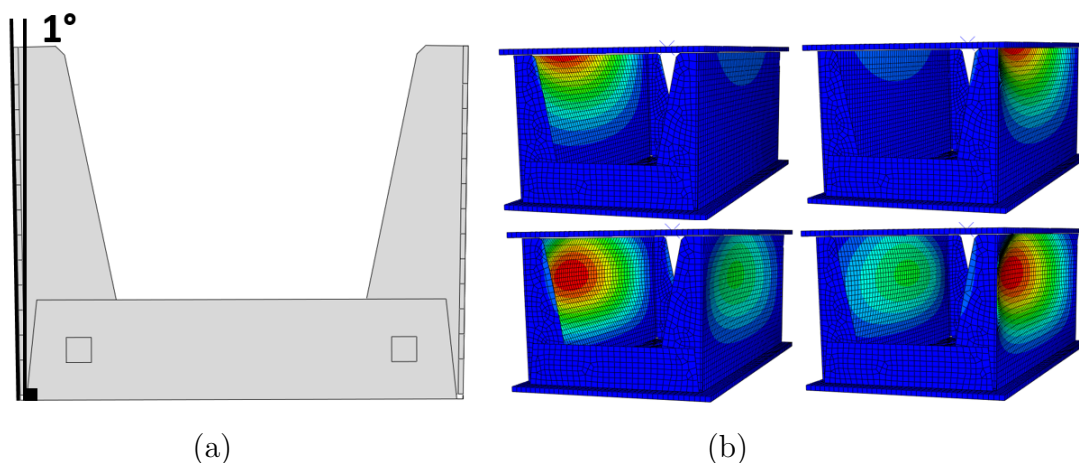


Figure 6.11: In picture (a) illustration of how the panels shifted  $1^\circ$  outwards. (b) the four buckling modes that were introduced as imperfections in the first step.

#### Material

There was not enough time to receive and test the material used in the compression test instead the material data was taken from an old (2005) feasibility study, the corrugated board is three layer consisting of:

- Outer liner: Euroliner D, testliner 4, whitetop 150g

- Fluting: Eurokemoionda, 225g
- Inner liner: Euroliner D, testliner 4, whitetop, 125g

The material properties presented in table 6.1 and 6.2 is given from the recycling mill Lucca.

Table 6.1: Effective material properties of the layers in the panel

Material	Outer Liner	Fluting	Inner Liner	Corrugated Core
$E_1$ [MPa]	3900 <sup>1</sup>	4540 <sup>1</sup>	4840	1 <sup>2</sup>
$E_2$ [MPa]	1610 <sup>1</sup>	1770 <sup>1</sup>	1770 <sup>1</sup>	329 <sup>3</sup>
$E_3$ [MPa]	10 <sup>4</sup>	-	10 <sup>4</sup>	10 <sup>4</sup>
$G_{12}$ [MPa]	969 <sup>5</sup>	-	1132 <sup>5</sup>	5 <sup>6</sup>
$G_{13}$ [MPa]	7 <sup>6</sup>	-	7 <sup>6</sup>	3, 5 <sup>6</sup>
$G_{23}$ [MPa]	70 <sup>6</sup>	-	70 <sup>6</sup>	35 <sup>6</sup>
$v_{12}$	0, 34 <sup>6</sup>	-	0, 34 <sup>6</sup>	0, 05 <sup>6</sup>
$v_{13}$	0, 01 <sup>6</sup>	-	0, 01 <sup>6</sup>	0, 01 <sup>6</sup>
$v_{23}$	0, 01 <sup>6</sup>	-	0, 01 <sup>6</sup>	0, 01 <sup>6</sup>

<sup>1</sup> Material properties given from feasibility study.

<sup>2</sup> According to Nordstrand  $E_{1,2} \approx 0$  [17].

<sup>3</sup> Calculated according to Nordstrand equation 3.1.

<sup>4</sup> Approximated.

<sup>5</sup> Calculated with Baums equation 3.4.

<sup>6</sup> Taken from Nordstrand [17].



Table 6.2: Effective material properties of the layers in the panel

Material	Outer Liner	Fluting	Inner Liner	Corrugated Core
Thickness [mm]	0, 23 <sup>1</sup>	0, 367 <sup>1</sup>	0, 17 <sup>1</sup>	2, 6 <sup>2</sup>
Thickness Crease [mm]	0, 23 <sup>1</sup>	-	0, 17 <sup>1</sup>	0, 2 <sup>3</sup>
Density [Tonne/mm <sup>3</sup> ]	5, 56E - 10 <sup>1</sup>	6, 14E - 10 <sup>1</sup>	6, 24E - 10 <sup>1</sup>	1, 14E - 10 <sup>4</sup>
Plasticity				
$\sigma_1^y$ [MPa]	14, 3 <sup>1</sup>	-	17, 02 <sup>1</sup>	14 <sup>1</sup>
$\sigma_2^y$ [MPa]	7, 15 <sup>1</sup>	-	8, 51 <sup>1</sup>	7 <sup>1</sup>
$\sigma_3^y$ [MPa]	6, 43 <sup>1</sup>	-	7, 66 <sup>1</sup>	6, 3 <sup>1</sup>
$\tau_{12}^y$	5, 72 <sup>1</sup>	-	6, 81 <sup>1</sup>	5, 6 <sup>1</sup>
$\tau_{13}^y$	3, 57 <sup>1</sup>	-	3, 5 <sup>1</sup>	4, 26 <sup>1</sup>
$\tau_{23}^y$	2, 14 <sup>1</sup>	-	2, 55 <sup>1</sup>	2, 1 <sup>1</sup>

<sup>1</sup> Material properties given from feasibility study.

<sup>2</sup> According to Secondary package specification.

<sup>3</sup> Approximated.

<sup>4</sup> Calculated with equation 3.5.

The model was a shell model and the material properties was applied as a composite.

### Tie Constraints

The flaps on the secondary package is glued together to resemblance this in the model tie constraints were used, see figure 6.11 (a) where the tie section is shown as rectangles on the panels.

### Corners

For easier foldability the corners had perforation. In the model this was neglected. The corners were model with a reduced material thickness, the top and bottom liners had their original thickness but the homogeneous core thickness was reduced from 2.6 mm to 0.2 mm, this was an approximation.

### Mesh

The mesh had a global seed of 6, in total there existed 7006 elements mostly consisted of S4R elements (6908) and some S3 elements (98) where the geometry was complexed.

## 6.7 Secondary Unit

### 6.7.1 Assembling

Within a secondary package fits 16 TRC packages. These are set in a pattern, shown in figure 1.3, with eight and two packages in the length- and width-direction, respectively. This is done in the assembly-module of ABAQUS.

During the real assembling of secondary unit a compression load in between the packages, caused by the dimensions of the secondary package, is initiated. This is to stabilize and prevent the packages of getting miss-aligned or fall out from the unit. This was observed during the physical tests and has been implemented in the FE-model. No specific measurements of the load was performed, instead it was assumed to be a magnitude of 55N since the packages then fitted into the secondary unit.

To obtain the initial compression load five rigid bodies were created, one wall for each side except for the top. Two walls for each short side, these were used with a specific amplitude to generate the compression load. Two walls for each long side were encastred and created to stabilize the products and preventing them to move in this direction. Lastly, one side for the bottom which were modeled mainly to maintain the integrity of the products but a small displacement condition had to been implemented. See the illustration of the setup in figure 6.12

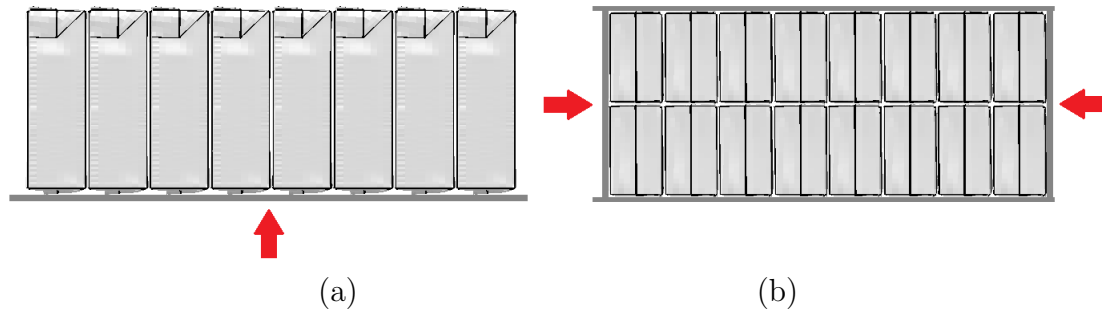


Figure 6.12: Picture (a) shows the the bottom plate and picture (b) the four rigid walls. The red arrows indicates how the rigid body plates moved along the different axes.

The contact properties had to be modeled carefully. Rigid bodies were not allowed to touch each other and had a frictionless surface to prevent the generation of unwanted surface traction. Between the packages there was a friction coefficient of 0.3. The geometry of the sixteen primary packages were, after the compression step, able to fit into the dimensions of a secondary package.

The next steps was to initiate the contact between the primary packages and the secondary package, then deactivate the contact of the rigid bodies and perform the top load analysis.

For future pallet simulation the efficiency of this process can be enhanced by 40 minutes per secondary unit. This is done by importing deformed ODB-geometries and by using a function called Predefined Fields where stresses, material and orientation is imported into the model. This makes it possible to only perform the compression load once and save hours in computing time when simulating pallets. To avoid large jumps and hourglassing after importing the stresses and strains an additional step were implemented. This was to make the big jumps, caused by the internal loads between the packages, much smoother. This was done according to Newton's second law  $F = ma$ , where the mass was enlarged using mass scaling to lower the accelerations.

All primary packages in the secondary package were modeled the same way as previous except for the top and bottom tie constraints these were excluded, see chapter 6.



# Chapter 7

## Top Load Compression Simulation

### 7.1 Introduction

In this chapter all the results from the simulations are presented and compared to the physical test results. The results are compared against each other for validation of the finite element models. The chapter is divided in subsections for easier separation of the different test. The simulated test is made to be identical to the physical test.

#### 7.1.1 Mass-scaling

All simulation results are done with mass-scaling  $10^{-6}$  to speed up the computational time. The results were compared with and without mass-scaling and there was no significant difference.

### 7.2 Primary Package Model

#### 7.2.1 Method

To evaluate the created models three different load cases were to be compared to the physical tests. This was to verify if all the assumptions and simplifications were reasonable. The setups, as mentioned in previous chapters, were a simple compression test, an unsymmetrical compression and an angled compression. All three setups are shown in figure 7.1

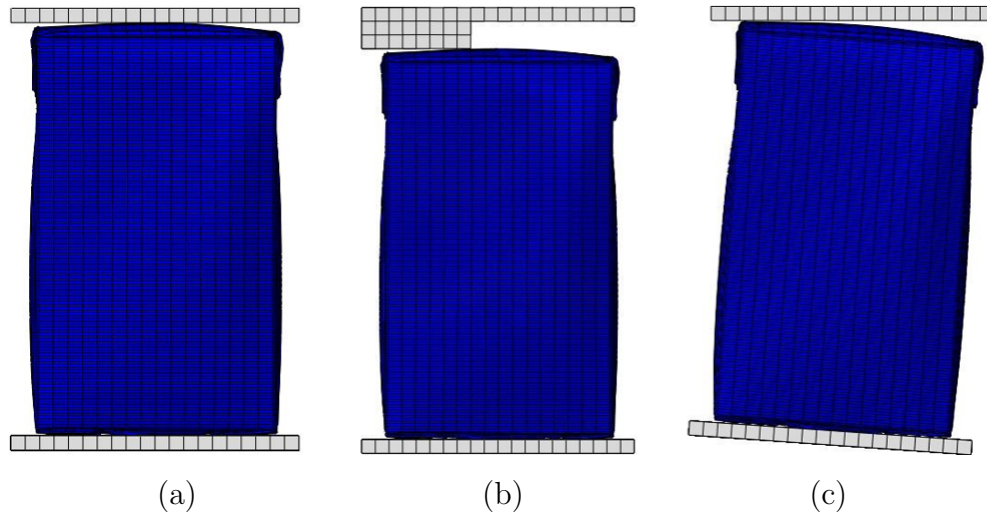


Figure 7.1: (a) illustrates Normal, (b) Unsymmetrical and (c) Angled compression.

### Test Parameters

The bottom plate was constrained as a Rigid Body and unable to move nor rotate in any direction. The top plate was modeled similarly with an exception for a translation velocity set to 50 mm/s along the negative vertical axis. The velocity of the top plate was initiated with a smooth step to avoid large impacts at high velocities.

All FE-simulations were run for 0.5 s and this results in a negative translation movement of 25 mm along the vertical axis.

Since the majority of the compression loads during transport are unsymmetrical along an axis, both the unsymmetrical load test and angled load test were chosen as test methods. This is of high interest to evaluate the differences in the maximum top load when the package exhibits a perturbation from the normal compression test. The unsymmetrical load test was modeled with a 9 mm solid extrusion on the left side of the top plate and in the angled load test both the bottom plate and the TRC package was rotated  $4^\circ$  in the y-direction.

## 7.2.2 Result

### Normal Compression

The buckling captured in the model resemblance the physical test, see figure 7.2 for a visualization. Figure 7.3 shows the force-deformation graph from the normal compression.



Figure 7.2: Shows the buckling behavior for the modified TRC package. Initial buckling is just below both flaps with an BCR at 180N and a Top plate displacement of 5.53 cm.

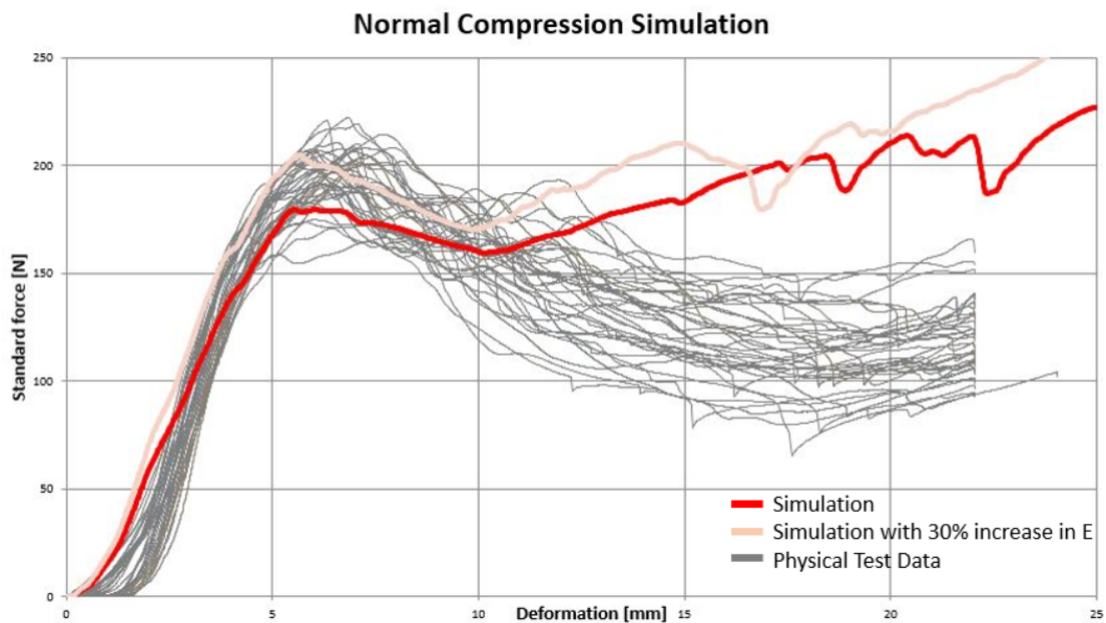


Figure 7.3: Shows the result from the symmetric compression analysis of the folded TRC package. The red line shows the regular compression simulation, pink is with an 30% increase of Youngs Modulus  $E$  in all directions and the grey solid lines shows data from the physical tests.

### Unsymmetrical

The buckling captured in the model resembles the physical test, see figure 7.4 for a visualization. Figure 7.5 shows the force-deformation graph from the unsymmetrical compression.



Figure 7.4: Shows the similarities of the buckling behavior in the model compared to the physical test.



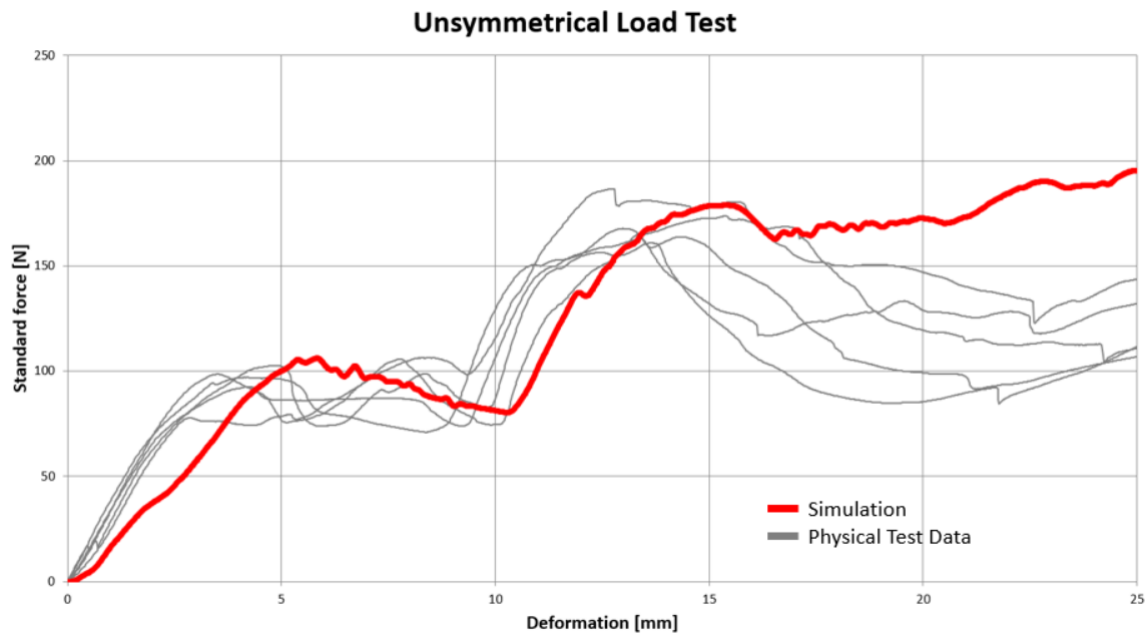


Figure 7.5: Shows the result from the symmetric compression analysis of the folded TRC package. Red is is the simulation and Grey are data from the physical tests.

### Angled

The buckling captured in the model resemblance the physical test, see figure 7.6 for a visualization. Figure 7.7 shows the force-deformation graph from the angled compression.



Figure 7.6: Shows the similarities of the buckling behavior in the model compared to the physical test.

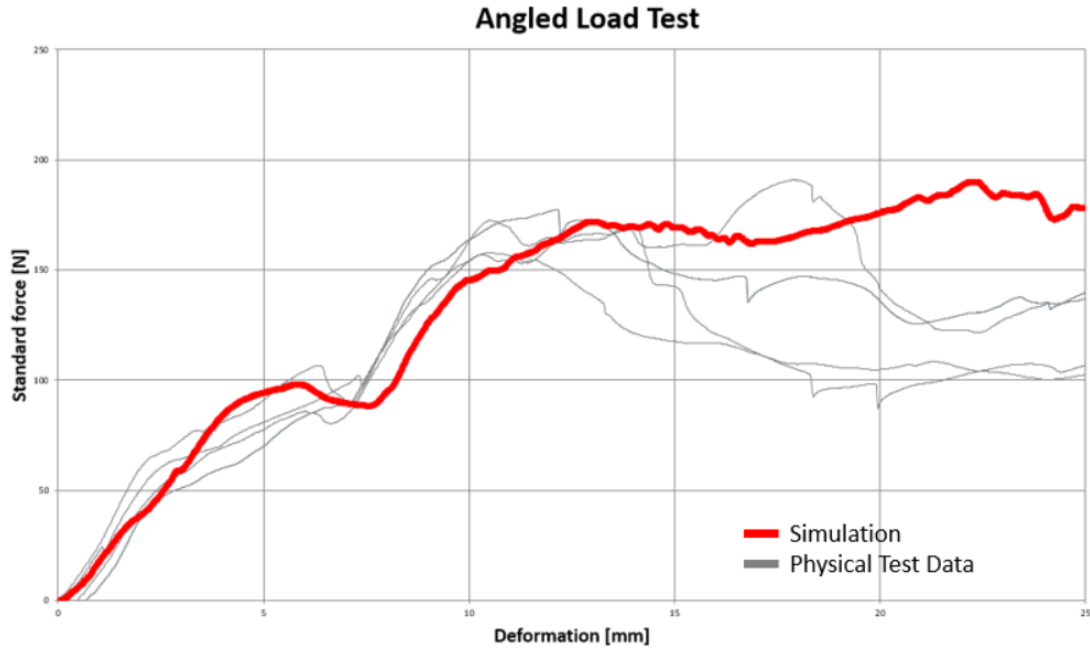


Figure 7.7: Shows the result from the symmetric compression analysis of the folded TRC package. Red is the simulation and Grey are data from the physical tests.

### 7.2.3 Analysis

#### Normal Compression

The compression simulation of the folded and modified TRC package shows a clear resemblance compared to the physical tests. The BCR is at 180N which is equal to the physical tests of the second buckling mode. The Buckling is initiated below the flaps on both sides which corresponds well to Buckling Mode 2, see figure 5.6. The geometry that triggers the first buckling mode was never investigated and therefore not captured in the simulations.

Different set-ups were used in the compression simulations. The results from this showed a large number of different buckling combinations and variety of the maximum load, this corresponds to the physical tests.

A small deviation in the resemblance between the simulation and the physical tests is the slope before the buckling, i.e the elastic zone. This could be caused by two reasons. Firstly, the chosen material data or secondly, that the models folding are not identical to the reality. This causes differences in the flap sealing and local imperfections. Same analysis was done for a 30% higher Young's Modulus  $E$  in all directions. The slope was then parallel to the physical tests with a higher BCR at 208,5N.

During post-buckling the applied force increases more rapidly than the physical tests, this is possibly a factor caused by unsuccessfully implemented cavity properties.

The simulations was done with a factor of  $10^{-6}$  in mass scaling, this was necessary to speed up the computational time with negligible differences. Higher factors of mass scaling were tried but the differences in the force-displacement curve and in the buckling illustration were to big to neglect.

### Unsymmetrical

The Force-Displacement Curve seems to fit the physical tests well. The BCR for the first and second buckling is is at approximately 100 and 150N, respectively. This corresponds well to the physical tests.

But similarly as in the Normal Compression Test the slope pre-buckling could be steeper to fit the curve even better. This was investigate for a 30% higher Young's modulus and is then parallel but with the two peaks at 120 and 195N.

### Angled

The test shows a resemblance for the model's buckling behavior during the compression analysis. The first buckling is initiated at just below 100N and the second one at approximately 160N.

Similarly as in the normal compression and in the Unsymmetrical Load Test the calibrated material used in the simulations are not as stiff as the material in the real TRC packages. Same evaluation was done for a 30% higher  $E$  in all directions.

Note that the measured angled in the physical tests were only constrained by the friction between the plates and the package. Possible sliding were possible but never observed by the eye.

## 7.2.4 Conclusions

The created FE-model seems to fit the physical tests well, especially the force-displacement curves. This is a verification that all assumptions and simplifications on the model were done in a reasonable manner. The physical packages compared to the folded models local imperfection are not identical, this could be the cause why the physical tests are has a steeper curve pre-buckling. This is believed to be possible by making simple adjustments to the geometry.

## 7.3 Secondary Package Model

### 7.3.1 Method

#### Test Parameters

The bottom plate was constrained as a Rigid Body and unable to move nor rotate in any direction. The top plate was modeled similarly with an exception for a translation velocity set to 40 mm/s in negative z-direction. The velocity of the top plate was initiated with a smooth step to avoid large impact forces at a high velocity.

All FE-simulations were run for 0.5 s and this results in a translation movement of 20 mm in negative z-direction.

The bottom section of the secondary package was constrained in all direction and rotation with a boundary condition, without this boundary condition the package bottom buckled. In the physical test the bottom was fixed down with weights to resemblance packages.

#### Assumptions

- Ideal plasticity is assumed in the outer and inner liner.
- Plasticity does not exist in the corrugated core. The correct data was not available, without plasticity the result graph looked more alike to the physical results.
- The thickness in the creases is reduced to 0.6 mm. Thickness of the two liners and the fluting together is 0.6 mm.

### 7.3.2 Result

The final material properties used in the model is seen in table 7.1, the bolded properties is the ones manipulated. The ideal plasticity in the outer and inner liner is reduced with 50% and the E moduli for the corrugated core is lowered to 105 MPa with trail and error test. The shear stress in the MDZD and CDZD was changed.

Table 7.1: Material properties used in the model

Material	Outer Liner	Corrugated Core	Inner Liner
$E_1$ [MPa]	3900	1	4840
$E_2$ [MPa]	1610	<b>105</b>	1770
$E_3$ [MPa]	10	10	10
$G_{12}$ [MPa]	969	5	1132
$G_{13}$ [MPa]	<b>70</b>	<b>35</b>	<b>70</b>
$G_{23}$ [MPa]	<b>7</b>	<b>3,5</b>	<b>7</b>
$v_{12}$	0,34	0,05	0,34
$v_{13}$	0,01	0,01	0,01
$v_{23}$	0,01	0,01	0,01
Plasticity			
$\sigma_1^y$ [MPa]	<b>7,15</b>	-	<b>8,51</b>
$\sigma_2^y$ [MPa]	<b>3,58</b>	-	<b>4,26</b>
$\sigma_3^y$ [MPa]	<b>3,22</b>	-	<b>3,83</b>
$\tau_{12}^y$	<b>2,86</b>	-	<b>3,41</b>
$\tau_{13}^y$	<b>1,79</b>	-	<b>2,31</b>
$\tau_{23}^y$	<b>1,07</b>	-	<b>1,28</b>

The buckling captured in the model resemblance the physical test, see figure 7.8 for a visualization.

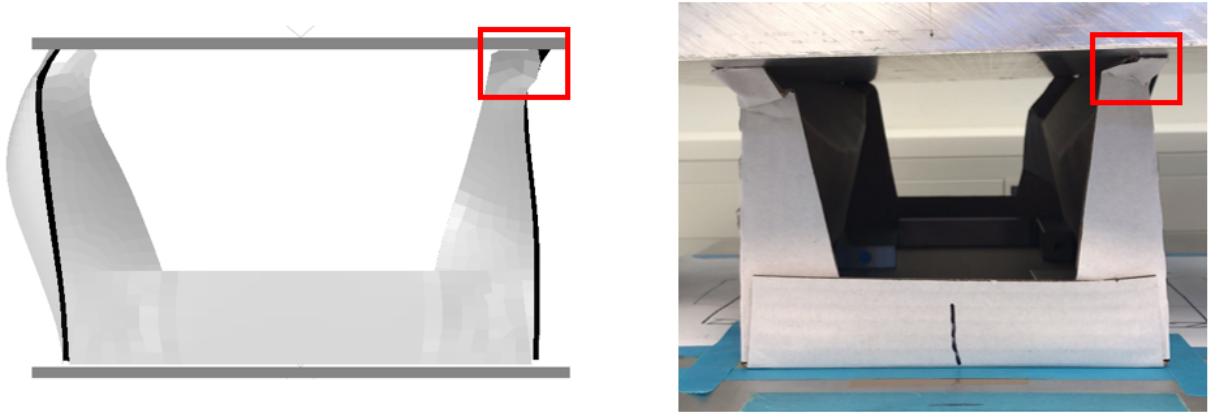


Figure 7.8: The right panel of the model is buckling inwards in accordance to the physical test. The left panel of the model is buckling outward, this buckling was identified in some of the physical test, however not in the physical picture presented. A figure with Von mises stress can be found in Appendix B.

In figure 7.9 the Green curve is representing the model of the secondary package, the model is compared to the physical tests (grey) and different versions of the model, described below. The model takes 29 minutes on 24 cores. The Yellow curve have the outer and inner liner material properties  $E_1$ ,  $E_2$  and  $G_{12}$  decreased with 50%.

In the Blue curve the perforation was added to the model i.e. where the perforation existed on the creases the material/surfaces was removed from the model.

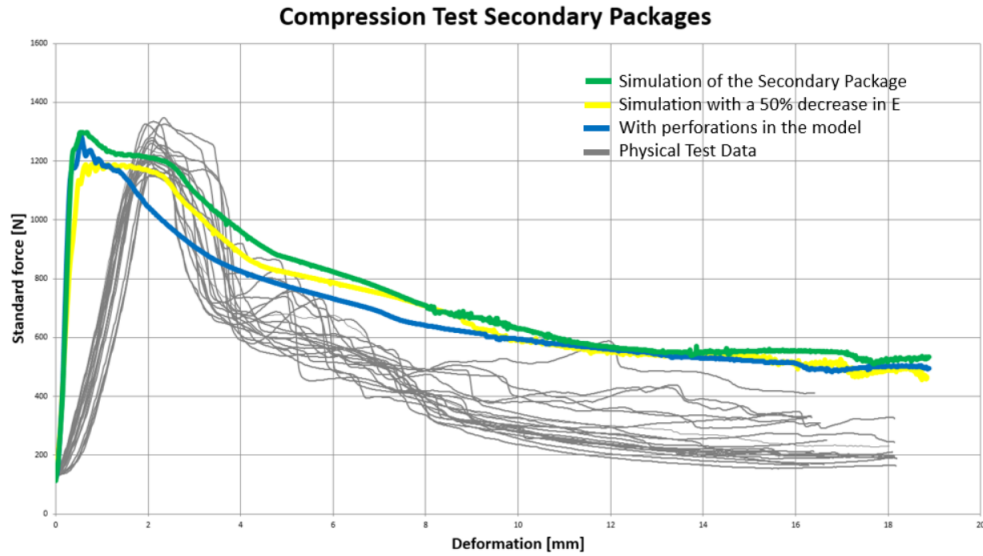


Figure 7.9: Force - displacement curve of normal compression of a secondary package with various test parameters.

### Limitations

- The material properties is received from tensile test and are not compatible with compression for an anisotropic material such as paper.
- Small local collapse is not captured by the model.
- The imperfections from the buckling analysis is not altering the geometry of the corners they are still "perfectly straight".
- The model is sensitive to material properties, geometry change, imperfections, mesh size and mass-scaling.

### 7.3.3 Analysis

The stiffness of the homogeneous core affects the BCR more crucial than the stiffness of the liners.

The model and the varieties of the model are too stiff compared to the physical test. The material properties is not really affecting the stiffness at all. The yellow curve have 50% lower stiffness but only a small change of incline is seen. In the physical test there were local collapse of the corners before the buckling, explaining the incline, this local collapse is not captured in the model.

The removal of the perforation in the model does not affect the BCR, but how the compression behave after the buckling, the result is consistent with the studied theory.

Plasticity is highly affecting the BCR and how the compression behaves after buckling, the plasticity parameters given is from tensile test and not compression test. The material parameters was not measured from the material still they could be used after they were trimmed to resemblance the physical tests.

### 7.3.4 Conclusions

The model chosen had the same BCR as the physical test. This was chosen to enable capturing the correct BCR for an assembled Secondary unit. Which is the next step in this thesis.

In a secondary unit with primary packages the headspace between secondary unit and packages is 3 mm, therefore the compression force was wanted to coincide with the physical test at that displacement, which it does.

After the buckling the model have a higher strength than the physical test but the behavior of the force-displacement graph is similar. The illustration of the buckling resemblance the reality and showed promising for the assembling of a full secondary unit.

## 7.4 Secondary Unit Model

### 7.4.1 Method

#### Test Parameters

The setup that were considered in the FE-simulations were in accordance to the physical tests. The top plate was measured to be tilted with an angle of  $3.2^\circ$  from an frozen image of the recorded movies. This was created in the FE-model and considered to be fixed through the entire top load analysis. A simulation without a tilt of the top surface was also performed and analysed. This was to be able to verify the created FE-model through a comparison between the simulations and the physical tests. An illustration of the setup is shown in figure 7.10. The extruded part from the top plate has the same geometry as the one in the physical test. Same test parameters were implemented as in the simulations for a primary package.

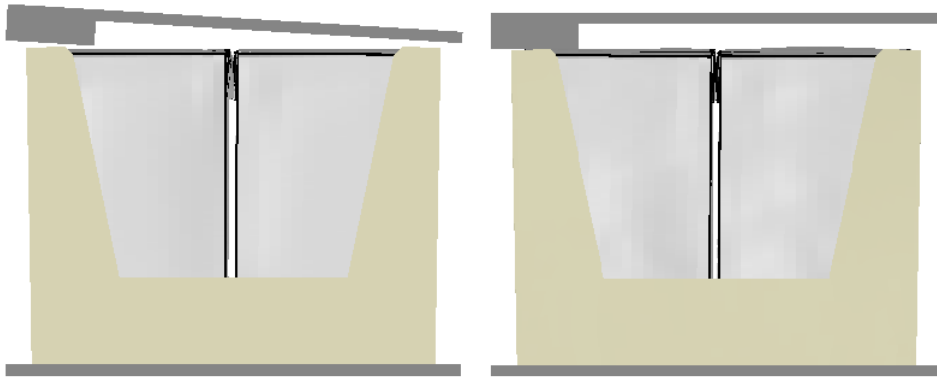


Figure 7.10: Illustrates the two load cases that were analysed in the FE-simulation.

## 7.4.2 Results

### Limitations

- All packages in the secondary unit is considered to have identical geometries
- The secondary unit was not folded. A similar folding procedure as for the primary model would be of interest
- The compression load is an approximate value set just to fit the packages inside the Secondary package
- The imperfections from the buckling analysis was not implemented on the secondary package
- The tilt of the top plate was measured from an image of the physical test

Figure 7.11 illustrates the resemblance of the physical test and the simulations. The secondary package is ripped apart in the corners under the metal bar. Figure 7.12 illustrates the same physical test and compression as in figure 7.11 but from the side. The red rectangles in figure 7.11 and 7.12 marks areas where the resemblance is high.



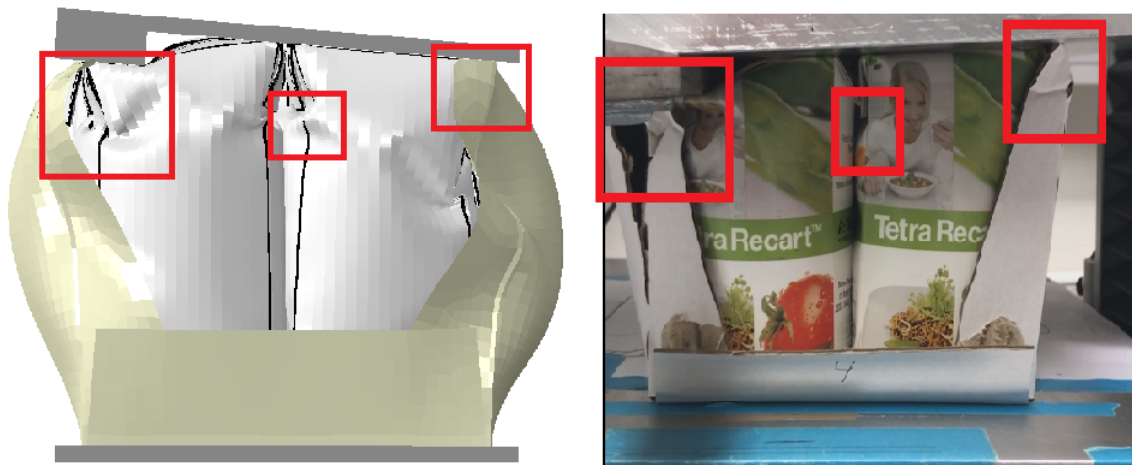


Figure 7.11: Illustrates how the buckling behavior of the simulations corresponds to reality. Each box showing different similarities.



Figure 7.12: Illustrates how the buckling behavior of the simulations corresponds to reality. The box shows a major similarity just below the flaps where the buckling is initiated.

In figure 7.13 is the four simulations compared to physical tests. Red is the simulation without a tilt with a mass-scaling of  $10^{-6}$  and the critical element along the

creases is scaled with a factor 10. Blue is the simulation when using Predefined fields and with a tilt. A mass-scaling of  $10^{-6}$  where used and the critical element along the creases is scaled with a factor 9.

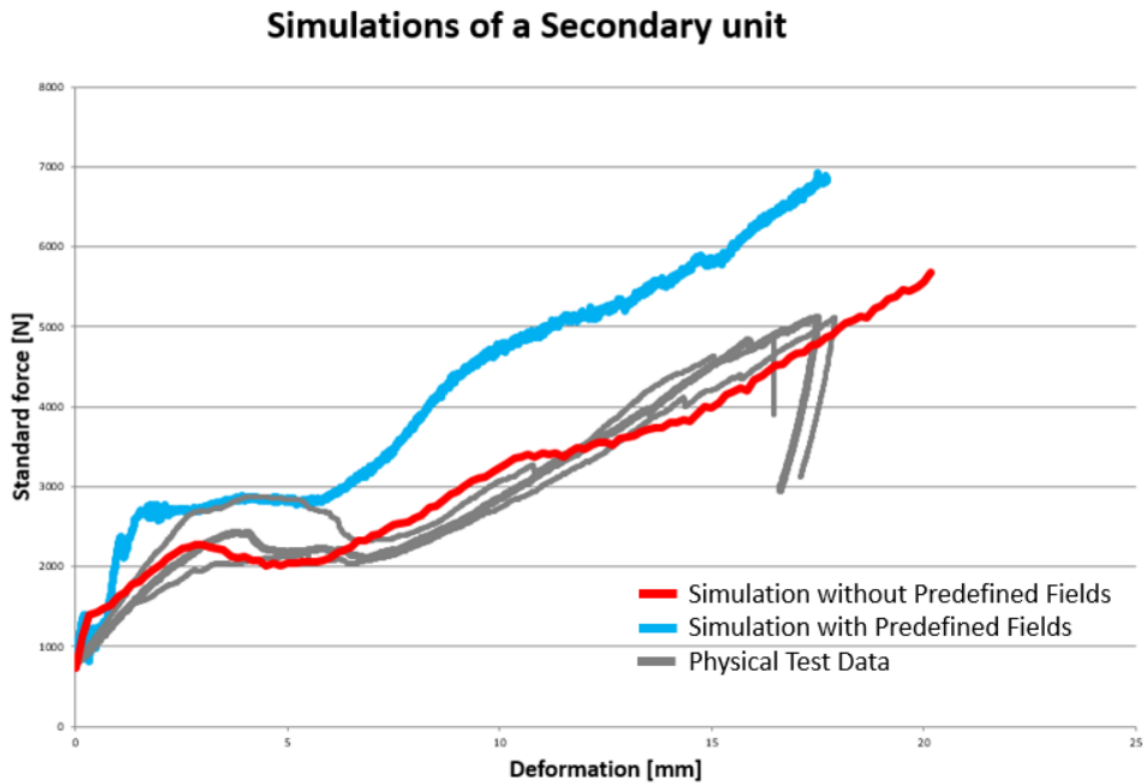


Figure 7.13: Shows the comparison between each setup and the physical tests with a tilted top plate. Grey curves are the physical test data, Red curve and Blue curve is without and with predefined fields, respectively.

### 7.4.3 Analysis

Both setups seems to capture the overall buckling behavior very well. In the physical tests the Secondary package is ripped apart in the left corners and the glue of the flap loosens its grip. This obviously affects the stability of the secondary unit. The FE-simulations did not capture this behaviour, in the simulations the corners and glue was intact. The two different approaches, with and without predefined fields, are discussed below. A verification of the stress field was never done and therefor not shown as a result. The obtained stress fields are presented in the appendix.

#### Without Predefined fields

The simulation without a tilted top surface is believed to be a bad comparison between the simulation and the physical tests. The reason for that is when the top is tilted the right side gets in contact and contribute to a higher BCR. The BCR is approximately 1200N lower for the simulation than the physical tests, this is due to the tilt.

By implementing the tilt the BCR will increase and the Force-Displacement curve of the simulations will coincide well with the physical tests, see the red curve above in figure 7.13.

Note that the tilt of the top surface through a physical test were not constant. But it appeared to be relatively constant until post-buckling of the secondary units left-side, therefor the surface were set to a fixed angled through the entire simulation.

The Compression and Top Load steps takes, on 24 cpu's, approximately 40 and 220 minutes, respectively. The compression step could be eliminated by assuming all secondary units contains identical packages with equal stress and strain distribution, i.e by using Predefined fields.

### **Predefined Fields**

When considering a Predefined Field the imported geometries will have an initial stress state. Therefor an initial and higher mass scaling was used to reduce high accelerations and big jumps when contact was inactivated. This process was done with a mass scaling of  $10^{-4}$  which was later reinitialized to  $10^{-6}$  before performing the top load analysis. This step was done in 2.5 minutes on 24 cpu.

It is clear from the blue graph in the Force-Displacement curve in figure 7.13 that the Secondary package is too stiff in the beginning, this phenomena was previously discussed. Due to the steep slope it causes the curve to be slightly pushed to the left compared to physical tests.

There are next to none differences in the buckling behavior which seems to be correctly captured for all setups. The Force-Displacement curve for Predefined Field seems to exhibit a higher external load at the same, this could be that equilibrium is not fulfilled in the initial state.

### **7.4.4 Conclusions**

The FE-model with no implementation of a predefined field is corresponding well to physical tests, both buckling behavior and the BCR. The simulation using a predefined field can exhibit a slightly higher load before buckling. The overall buckling behavior is correctly captured just below the flaps which was observable from the physical experiments.



# Chapter 8

## Discussion and Conclusions

### 8.1 Summary of thesis

The FE-model of the Primary package seems to behave in an accurate way compared to physical tests of mode 2. The BCR of the model is 180N which is almost identical to the physical tests. The Top Load Analysis of the secondary unit seems to capture the major and minor buckling behaviors and the Force-Displacement curve corresponds well to physical tests.

Assembling a Finite Element Model, verified by physical tests, of a Secondary unit from a folded Primary Package has not previously been performed at Tetra Pak. Thus, this thesis contributes to well-explained information of how the primary package behaves on its own and assembled in a Secondary package. The model corresponds well to physical tests and could be of interest to use in Pallet distribution tests in the future. The FE-models can be used to investigate how different parameters affect the packages BCR.

This thesis has presented the importance of how the geometry is modeled in a FEM software, if only the macro-structural behavior is of interest a material model capturing the anisotropic plasticity in tension such as Hill can be used.

The FE-models have not been evaluated if the tensile and compression tension received from the result is of comparable magnitude to the physical test.

### 8.2 Measurements discussion

The result from the measurements are reasonable and are considered to be accurate, but to minimize sources of errors, it is suggested that;

- When the TRC packages are manufactured at costumers the packages are air-dried standing vertical allowing the package to develop another geometry than the one tested in this thesis. The time from manufacturing to transportation on

a pallet also give space for geometry change. Recommendations is to identify these differences and investigate them with compression test and 3D-scan.

- The tilted top compression plate during the physical tests of the Secondary unit could be eliminated by setting the Unsymmetrical load (the metal bar) just below the ball-bearing.
- Both the primary package and the secondary package have a variety in height this affects were the Zwick instrument starts to measure. A specification of were the measurement should start is useful to receive comparable data.
- Two buckling modes were identified on the primary package with a difference in BCR value. The standard distribution can be more representable if it was divided into two distributions. More test results will lead to a more accurate distribution.

## 8.3 Modelling discussion

The FE-Model and the simplifications made corresponds well to the physical tests. But to obtain better corresponding simulation results improvements and adjustments is suggested and divided into primary and secondary package.

### Primary Package

In the beginning of this master thesis a "perfect" package model was designed, the model had a geometry with high resemblance to the reality but with straight corners. These straight corners did not allow the package to compress or to have small structure collapse resulting in a very stiff model before the initial buckling.

With the folding procedure the history and the geometry of the corners was captured and the received model had a stiffness more alike to the reality. However the folding model was highly sensitive, by refining and improving the folding several improvements would be made to the primary package model. Some examples of improvements to the folding are;

- An extra step during the sealing of the package blank to initiate the contact with a higher accuracy.
- The folding of the flaps is different in the top and bottom, the rotation of the flaps in the bottom showed most promising result.
- The geometry of the inner plates to be redesigned to allow the package panels to be pressed inwards under the flaps.
- Increase the total time of the folding procedure.
- A higher mass-scaling can be used, because only the extraction of the geometry is wanted.

- The cavity needs to be remodel, suggestion is to move the reference point and adding two extra reference points to eliminate overlapping of elements.
- Adding the mass-flowing step and the geometry change step for a complete model.

The source of errors in the primary package model that are in direct correlation with the folding would be eliminated if some of these suggestion would be implemented. Examples to direct improvements are;

- The geometry of the model.
- The mesh could be refined, lowering the current mesh length-width ratio.
- The cavity within the package would be fully enclosed. This has, in the simulations, been considered as an open surface which is not correct.
- Different material models can be tested.
- A buckling analysis could be performed introducing imperfections, this could trigger the first buckling mode. The geometry of a primary package has great affect on the deformation pattern. With several packages with different geometry assemble in a secondary package are more representable to the reality.

Even with all the limitations and source of errors listed above information from the model could be found.

- The headspace in the package or the volume difference does not affect the packages BCR, both these parameters affects the cavity definition and this statement could be false in respect to the unclosed cavity.
- Changing the material properties affects the package's BCR.

## Secondary Package

Without the correct material data for the corrugated cardboard used in the physical test the validation of the model is impossible. The secondary package showed same responses as the first "perfect" primary package model, the secondary package was modeled with straight corners making it too stiff.

The behavior after buckling is not fully captured in the model even by manipulation the material parameters. One material parameter that could be tested accurately is the compression stiffness in ZD-direction.

## Secondary Unit

In the physical test the flaps was torn away and the corners was rip open, none of this happenings was captured in the model. The glue constrain in the model can be assigned a maximum force before deactivating it. In the corners a XFEM analysis could maybe be implemented [27].

## 8.4 Future work

- **Improve the folding procedure** - See the discussion of the primary model above.
- **Perform more compression test on secondary unit** - Compression plates without a ball bearing is of interest to use to achieve a vertical compression, with more test result the validation of the model is easier to compare with the physical buckling. It is of interest to increase the Zwick instrument max force to well above a 6kN force limit, this would ensure capturing a full normal compression.
- **Analysis of corrugated board material properties** - Perform compression and tensile test on corrugated board used for TRC secondary packages.
- **Folding Model for the secondary package** - One suggestion for a standardize approach is to construct a model for folding of a secondary package. The model get a more realistic geometry and the stiffness is likely to decrease. The buckling analysis can therefore be neglected.
- **Material models** Test other material models such as XIA[28] and EBT[29]. What physics can the XIA material model capture, when considering differences in tension and compression? Can the EBT material model capture any delaminations that the HILL material model doesn't?
- **Investigate tension before failure** The finite element model is not evaluated if the compression and tensile tension is of comparable magnitude, this needs to be validated with physical tests.



# Bibliography

- [1] Tetra Pak processing and packaging solutions for food and beverages. [ONLINE] Available at: <http://www.tetrapak.com>. [Accessed 10 February 2018].
- [2] Tetra Pak - Tetra Recart Internal web page. [ONLINE] Available at: <http://www.intranet.tetrapak.com>. [Accessed 10 February 2018].
- [3] 55.180.40- Complete, filled transport packages. [ONLINE] Available at: <https://www.iso.org/ics/55.180.40/x/>. [Accessed 15 March 2018].
- [4] ASTM D4169 - 16 Standard Practice for Performance Testing of Shipping Containers and Systems. 2018. [ONLINE] Available at: <https://www.astm.org/Standards/D4169.htm>. [Accessed 16 March 2018].
- [5] J. Lönn, J. Navréd, 2006. Drop Test of a Soft Beverage Package Experimental Tests and a Parameter Study in Abaqus. Master Dissertation. Sweden: Lund University.
- [6] Hill, R. 1948. A theory of the yielding and plastic flow of anisotropic metals. Proc. Roy. Soc. London, 193:281-297
- [7] Östlund, S., Mäkelä, P. 2003. Orthotropic elastic-plastic material model for paper materials. International Journal of Solids and Structures, [Online]. 40, 5599-5620
- [8] Mäkelä, P. and Tryding, J. 2013. Evaluation of the performance of the Fortuna Splitting Machine in multiply paperboard splitting applications, DR28009, Tetra Pak.
- [9] Baum, G. A., Brennan, D. C. and Habeger, C. C. 1981. Orthotropic Elastic Constants of Paper, Tappi Journal 64(8), 97-101.
- [10] Stenberg, N. and Fellers, C. 2002. Out-of-plane Poisson's ratios of paper and paperboard, Nordic Pulp and Paper research Journal 17(4), 387-394.
- [11] T. Belytschko, Wing Kam Liu & Brian Moran Nonlinear Finite Elements for Continua and Structures, Wiley 2001.
- [12] Abaqus 2016 Documentation. [ONLINE] Available at: <http://50.16.225.63/v2016/>. [Accessed 15 March 2018].

- [13] Korin, C., Ristinmaa, M., Saabye Ottosen, N, Analytical prediction of package collapse - Consideration of windows in the package. Nordic Pulp and Paper Research Journal, Volume 29, Issue 4, 2014, Pages 717-724
- [14] Mäkelä, P and Fellers, C. 2012. An analytic procedure for determination of fracture toughness of paper materials. Nordic Pulp and Paper Research Journal, 27 no.2/2012, 352-360.
- [15] Internal Report - Muzzi, S. and Tryding, J. 2009. Box Compression Resistance (BCR) of TBA packages: evaluation of a model to predict package collapse, Tetra Pak AB.
- [16] Alfthan, J. and Tillander, O. and Trost, T. and Tysén, A. and Kihlstedt, A. 2012. Failure due to perforation in corrugated board boxes Influence on the box compression test, Innventia Report No: 381
- [17] Nordstrand, T. M. 1995. Parametric Study of the Postbuckling Strength of Structural Core Sandwich Panels. Composite Structures, 30, 441-451
- [18] Baum, G. A. and Brennan, D. C. and Habeger, C. C. 1981. Orthotropic elastic constants of paper. TAPPI PRESS, Vol.64, No. 8.
- [19] Ottosen, N. S. and Ristinmaa, M. 1999. The Mechanics of Constitutive Modelling, Volume I-II, Division of Solid Mechanics, Lund University.
- [20] A. Harrysson, M. Harrysson & M. Ristinmaa Current Models for Paper and Paperboard, Division of Solid Mechanics, Lund University, 2003.
- [21] Magnusson, A. and Nyman, U. and Ristinmaa, M. 2007. Elasticplastic properties of creases; testing, calibration and modelling. Status report.
- [22] ATOS Core - GOM. 2018 [ONLINE] Available at: <https://www.gom.com/metrology-systems/atos/atos-core.html>. [Accessed 05 April 2018].
- [23] ProLine by Zwick - for standardized tests. 2018 [ONLINE] Available at: <https://www.zwick.com/en/universal-testing-machines/proline>. [Accessed 05 April 2018]
- [24] Zetterqvist, L. and Lindström, J. 2017. Räkna med variation. 1st Edition. Studentlitteratur AB, Lund.
- [25] Internal Test Method - I021.43 Top Compression. 2015, Tetra Recart.
- [26] Internal calibration - MD0020 Testing & Calibration of Tetra Recart. 2012, DSO
- [27] Simulia XFEM Analysis Abaqus [ONLINE] Available at: <http://www.simulia.com/download/rum11/UK/Advanced-XFEM-Analysis.pdf> [Accessed 30 May 2018].

- 
- [28] Xia, Q. 2002. Mechanics of inelastic deformation and delamination in paperboard, Massachusetts Institute of Technology
  - [29] Borgkvist, E. Continuum modelling of the mechanical response of paper-based materials, Division of Solid Mechanics, Lund University, 2016



# Appendices

# Appendix A

## Model data

### A.1 Bulk modulus

Table A.1: Effective material properties of the layers in the panel

Material	Density at 25°C [Tonnes/mm <sup>3</sup> ]	Bulk Modulus [MPa]
Air	1,2E-12	0,101
Water	9,97E-10	22000
Calculated TRC data <sup>1</sup>		
Cavity	9,49E-10	2,07

<sup>1</sup> The total volume of the package model was 514 ml, therefore the headspace calculated was 25 ml to receive the 11 ml headspace specified. Equation 6.1 were used.

# Appendix B

## Pictures

### Primary Package

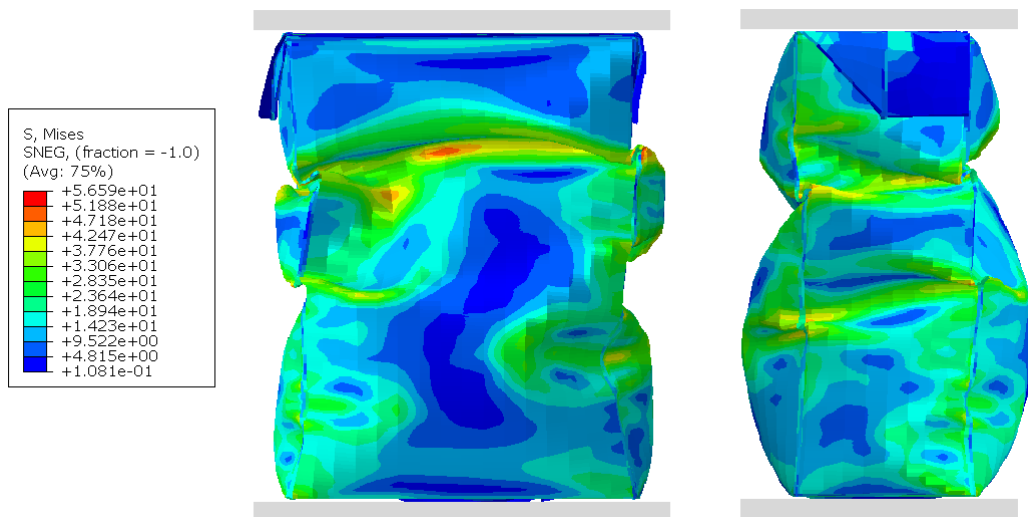


Figure B.1: A visualisation of the stress-distribution of the deformed primary package

## Secondary package

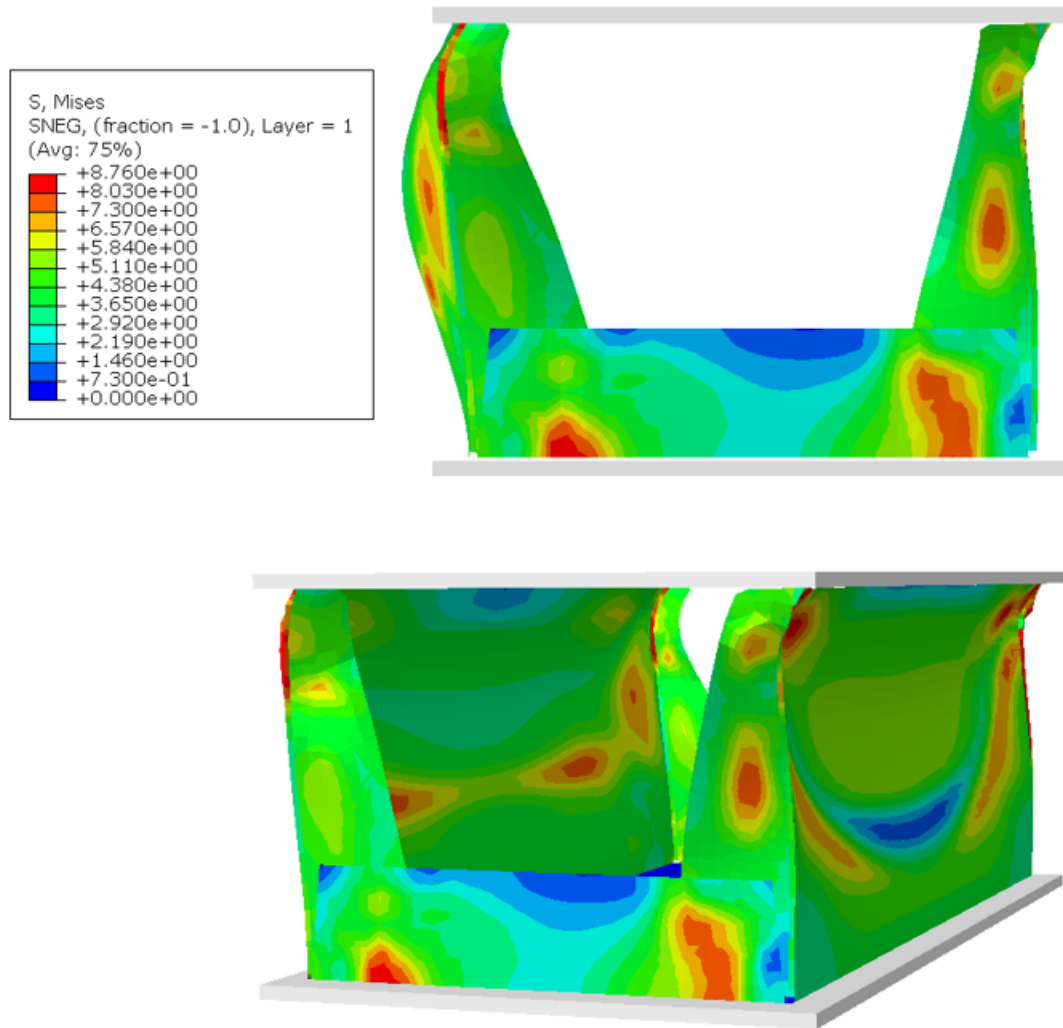


Figure B.2: A visualisation of the stress-distribution of the deformed secondary package



## Secondary Unit

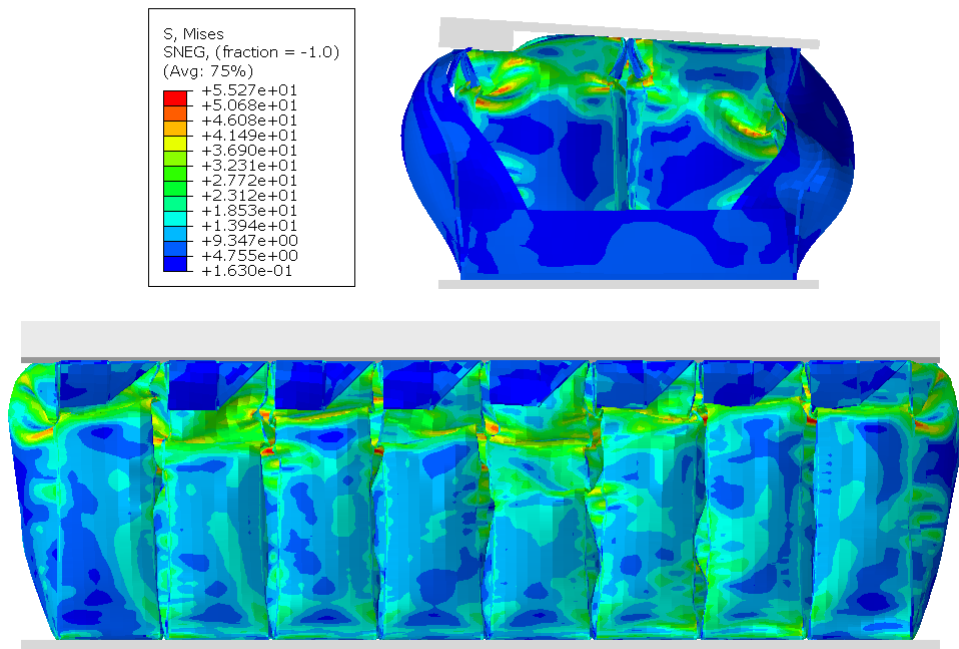


Figure B.3: A visualisation of the stress-distribution of the deformed Secondary Unit.